UC Irvine
UC Irvine Electronic Theses and Dissertations

Title
Investigation of Mixed Reagents on the Extraction of Lanthanides from Used Nuclear Fuel

Permalink
https://escholarship.org/uc/item/26j465td

Author
Moon, Jisue

Publication Date
2018

Peer reviewed|Thesis/dissertation

UNIVERSITY OF CALIFORNIA,
IRVINE

Investigation of mixed reagents on the extraction of lanthanides from Used Nuclear Fuel

DISSERTATION

submitted in partial satisfaction of the requirements
for the degree of

DOCTOR OF PHILOSOPHY

in Chemical Engineering

by

Jisue Moon

Dissertation Committee:
Professor Mikael Nilsson, Chair
Professor A. J. Shaka
Professor Shane Ardo

2018

DEDICATION

To

My family, friends and all those who have guided me along the way

TABLE OF CONTENTS

Page

LIST OF FIGURES

LIST OF TABLES

ACKNOWLEDGMENTS

I would like to express my sincere gratitude to my advisor Professor Mikael Nilsson for the support of my Ph.D study and research. My research would have been impossible to present my achievement in this thesis without the aid and support of him. I would also like to appreciate my committee members, Professor A. J. Shaka and Professor Shane Ardo. I would also like express my gratitude to Dr. Mark Antonio who has guided X-ray experiments at APS. It has truly been an honor working with him. I would like to thank the UCI TRIGA® Reactor Facility and Dr. George Miller for his help and support with reactor runs. I am also profoundly grateful to Dr. Carter Abney who gave me a chance to work at Oak Ridge National Laboratory. Without his support, I could not get a chance to learn variety of experimental skills at the national laboratory.

All the way through my PhD degree, all friends have been there for me. Rose, Kara, Christian, Tro, Randy, Leila, Quynh, Edward, Alan, Jonathan, Andy, Ted, Raul and Jackie provided advice and help throughout the years. They have been the best colleagues that anyone could hope for and will be greatly missed.

My parents and family have been the most important support group for me as I have been working on my PhD. I would not be able to finish degree without the unconditional love and support from my family. The biggest thank and heart goes my husband Alex for the love and joy we have shared and will continue.

CURRICULUM VITAE

Jisue Moon

2013   B.A. in Chemical Engineering, Dankook University, South Korea

2015   M.S in Chemical Engineering, Dankook University, South Korea

2018   Ph.D. in Chemical Engineering, University of California, Irvine

FIELD OF STUDY

Synergistic solvent extraction investigation of mixed extractants system for used nuclear fuel processing

PUBLICATIONS

1. Ji-Sue Moon, Mark Antonio and Mikael Nilsson, Influence of ionic medium on extraction of lanthanides by AOT reverse micelles (Under review, J. Phys. Chem. B)
2. Ji-Sue Moon, and Mikael Nilsson, Coordination chemistry of lanthanides extraction by AOT-CMPO reverse micelle; XAFS and UV-Vis study (Under review, Dalton transaction)
3. Ji-Sue Moon, Mark Antonio and Mikael Nilsson, A SAXS study of Aggregation in the AOT-CMPO solvent extraction system (In preparation)
4. Hui Ynag, Chen Xing, Guoxiang Hu, Siobhan J. Bradley, Jisue Moon, Xin Wu, Feng Guo, Thomas Nann, Carter W Abney, De-En Jiang, Shane G. Telfer, He Tian, Jian Zhang, and Shengqian Ma, A General Approach to Atomic Iron Sites Dispersed in N-doped Carbon Capsules for Electrocatalytic Hydrogen Evolution (Under review, Angewandte Chemie)
5. Hui Yang, Chen Xing, Guoxiang Hu, Siobhan J. Bradley, Jisue Moon, Xin Wu, Feng Guo, Thomas Nann, Carter W Abney, De-En Jiang, Shane G. Telfer, He Tian, Jian Zhang, and Shengqian Ma, Atomic Iron/Nitrogen-Embeded Hollow Porous Carbon Capsule as Superior Hydrogen Evolution Reaction Electrocatalyst (Under review, JACS)
6. Yue Nan, Seungrag Choi, Carter W. Abney, Jisue Moon, Jiuxu Liu, and Lawrence L. Tavlarides, Degradation mechanism of Ag mordenite in nuclear fuel reprocessing off-gases including air, H_2O and NOx (In preparation)
7. Jisue Moon, andMikael Nilsson, "Investigation on the Properties of Micelle and Reverse Micelle in Water/AOT/Heptane System for Holmium Extraction", GLOBAL, South Korea, September 2017

ABSTRACT OF THE DISSERTATION

Investigation of mixed reagents on the extraction of lanthanides from Used Nuclear Fuel

By

Jisue Moon

Doctor of Philosophy in Chemical Engineering

University of California, Irvine, 2018

Professor Mikael Nilsson, Chair

The fission and neutron capture reaction occurring in nuclear reactors generates a waste stream which includes more than 40 elements across the periodic table. The chemical separation of metal ions by liquid-liquid extraction from an aqueous phase into an organic phase is an important technology for purifying, recycling or disposing of solutions from metallurgical or nuclear industry. In recent studies, the extraction of the metal ion into microemulsion containing an anionic surfactant and an electrically neutral organic ligand (extractant) has been introduced as a new technology.

In this study, we applied an anionic surfactant to understand better the mechanism of liquid-liquid extraction under microemulsion-forming conditions. Aerosol OT (AOT) is well used as an anionic surface-active agent to form a microemulsion but it is not used alone in extraction systems because of poor extractability, and poor selectivity for lanthanides in their extraction from aqueous nitric acid solutions. It is known that the separation of lanthanides is considerably improved by using the combination of AOT and neutral extractant such as CMPO or bulky diamide, but the mechanism of the extraction remains

unclear. The aim of this research is to understand the extraction mechanism of an extraction system combining AOT and CMPO using various aqueous conditions and by analyzing the coordinate environment surrounding the extracted metal ion. A variety experimental technique including UV-vis-NIR, X-ray scattering and absorption spectroscopy, have been employed to gain a thorough understanding of the system. I will discuss the findings and their implementations on the extraction process of lanthanides from acidic environments.

CHAPTER 1: INTRODUCTION AND BACKGROUND

1. 1   Introduction

Nuclear energy is the leading electricity production method for low carbon power generation. In nuclear power plants, neutrons collide with uranium atoms, splitting the atoms and causing the release of additional neutrons that in turn collide with other uranium atoms resulting in a chain reaction. This produces various fission products from germanium to erbium. The majority of fission products have an excess number of neutrons than what is required for stability, and therefore undergo β^- decay until they attain stability[1-2].

From the fission, a significant amount of the lanthanide elements are produced, which is the group of elements in the sixth period of the periodic table: Lanthanide (La), Cerium (Ce), Praseodymium (Pr), Neodymium (Nd), promethium (Pm), Samarium (Sm), Europium (Eu), Gadolinium (Gd), Terbium (Tb), Dysprosium (Dy), Holmium (Ho), Erbium (Er), Thulium(Tm), Ytterbium (Yb) and Lutetium (Lu)[3]. Lanthanides have special electron configuration where a deeper lying orbital, the so called 4f orbital, accommodates new electrons. Because of this, the ionic radii become smaller with increasing atomic number. In addition, the lanthanides have a wide range of coordination number generally from 6 to 12. Due to their diverse properties, they are very useful for a wide range of applications. They play an essential role in modern technologies such as permanent magnets in automobiles, computers, alternative energy turbines, rechargeable batteries, catalysts, phosphors in lamps and plasma screen and other applications. Especially, neodymium has been used to

create permanent magnet alloys and also used as a catalyst for petroleum refining to produce useful oil from the residue of the crude oil[4]. Over the last decades, more than 90 % of the supply of the rare earth elements have been provided by mining operation in China. Because of this high dependency on China and a drastically increasing demand for rare earth elements, the price increases and a supply risk is serious concern[5-6].

In addition to the fission reaction, a neutron capture reaction also occurs and produces other higher atomic number transuranic elements. Plutonium and minor actinides (MA) which include neptunium, americium, curium and small quantities of higher actinides account for about 1 % of the total mass of used nuclear fuel (UNF). However, these elements emit alpha particles, which have high radiation energy, and in addition these elements often have a long decay chain and/or long individual half-lives, often with additional alpha emissions, before achieving permanent stability. This highly energetic decay makes transuranic elements a primary radiotoxicity source for the nuclear waste[7].

The principal method for used nuclear fuel (UNF) reprocessing to separate lanthanides and actinides from the waste stream is solvent extraction (SX). SX facilitates transport of desired solutes between two immiscible aqueous and organic phases using selective extraction reagents. The separation occurs due to the difference of affinities for certain solutes (such as metal ions) present in the aqueous phase, to chosen extraction reagents in the organic phase. In short, extraction reagents make solutes of interest more hydrophobic and therefore soluble in the organic phase while other solutes are left behind in the aqueous phase. In the context of UNF reprocessing, solutes of interest include uranium, plutonium, MA and some FP, with the goal being that each solute of interest or group of solutes can be extracted selectively from the others. An example of such a process

employed for reprocessing spent fuel is the PUREX (Plutonium/Uranium Reduction by EXtraction) process which relies on tri-n-butyl phosphate (TBP) to selectively extract U and Pu away from the fission and corrosion products as well as the minor actinides[8]. More recent studies have looked into combining two or more extractants into a single solvent to achieve separations in single-step processes for selectively extracting transuranic elements. For example, TRUSPEAK (Transuranic Separation by Phosphorus-reagent Extraction from Aqueous Komplexs) is a process that uses a combination of octyl(phenyl)-N,N-diisobutyl carbamoylmethylphosphine oxide (CMPO) and bis-(2-ethylhexyl)phosphoric acid (HDEHP) to extract transuranic elements away from the lanthanides[9].

In addition to using mixed extractants, reversed micellar extraction has been studied for selective extraction of certain solutes. This extraction has been used intensively in the biochemical field[10-11] and also used as a novel technique for the extraction of metals especially in the viewpoint of catalyzing metal reactions in the organic phase[12-13]. The reverse-micelle extraction has a great potential to create a new process of high performance extraction of metal ions for the treatment of used nuclear fuel. While recent studies have been conducted to show the improvement of extractability by adding different neutral extractants, there is a lack of studies that show how the reverse micelle or the neutral extractant affects the extraction[14]. For example, Aerosol OT (AOT) which has a double-chained anionic surfactant known to form microemulsions, but it forms massive emulsion in the interface of two phases at higher concentration. However, this can be solved by adding a small amount of CMPO. The fact that CMPO itself is not surface active

and thus does not work as a cosurfactant to form mixed reversed microemulsion seems very important, but it is not well understood why this improvement happens.

In this thesis, I investigated how a combination of AOT and a neutral extractant in an extraction system for metal ions affects to the solute extractability and the phase stability. Holmium and erbium were chosen due to their spectroscopic properties that include hypersensitive bands responsive to the coordination and geometry of the surroundings. Water, metal ion and nitric acid extraction were carefully monitored as a function of AOT to neutral extractant concentration ratio. Additionally, the nature of the complexes formed in the organic phase was investigated through use of UV-Vis-NIR.

In addition to the UV-Vis spectra, X-ray absorption fine structure (EXAFS) and X-ray absorption near edge structure (XANES) was applied to investigate the nature of the reverse micelles and the complexes formed in the organic phase. Also, small-angle x-ray was adapted to investigate the structure and interactions between reverse micelle aggregates to explain the relationship between reverse micelle and third phase formation. The findings in this study thus far provide some possible explanations on the synergistic extraction effect combining acidic and neutral extraction reagents as well as providing some hints on how supramolecular aggregates in the organic phase affect the solvent extraction systems.

1.2 Solvent Extraction

Solvent extraction is usually used in laboratory and process industry to selectively remove a targeted material from an aqueous phase into on organic phase by contacting these two immiscible phases. Because of its speed and simplicity, this process is often the

preferred separation method for non-volatile solutes. The extraction selectivity and the extractability is variable depending on the extractant properties, system compositions and diluent properties. After contact of the two immiscible phases, a sample may be taken from each phase to analyze the distribution of the metal between the phases. For metal species M, the distribution ratio, a measure of how well extracted a species is, can be written as:

$$\boldsymbol{D_M} = \frac{Concentration\ of\ all\ species\ containing\ M\ in\ organic\ phase}{Concentration\ of\ all\ species\ containing\ M\ in\ aqueous\ phase} = \frac{[M]_{t,org}}{[M]_{t,aq}} \tag{1.1}$$

In the nuclear field, solvent extraction has played a very important role in the waste processing. It started in the early 1950s to recover uranium and plutonium for national weapons programs through the PUREX process (plutonium uranium reduction extraction). In the early days of the used nuclear fuel processing carried out at Oak Ridge National Lab, TBP and other similar neutral organophosphorous compounds were investigated extensively and ultimately were used to replace ethers and ketones for the raw material processing and the nuclear fuel processing.

The complexes containing metals can be classified according to the type of ligand and these classes are summarized in table 1[15]. N refers to the maximum coordination number of the metal relative to the ligand.

Table1.1 Extraction complexation model classification

Class	Description	Example
A	Extraction of simple inorganic molecules	$MX_N = GeCl_4$
B	Neutral complexes between a metal ion and a lipophilic organic acid(z=N/2)	$MA_Z = Th(RCOO)_4$

C	Neutral complexes between a metal ion and a ligand. The complexes are unsaturated and can accept uncharged organic molecules or solvating agents (N>z or 2z)	$ML_zB_b = (UO_2)(NO_3)_2(TBP)_2$
D	Ion pair extraction. An anion or a cation exchange mechanism takes place	$Q^+L^- = R_3N^+Cl^-$
E	Other extractions	Crown ethers, etc

These types of extractants are cation exchangers (or acidic extractants), solvation extractants (or neutral extractant), and anion exchangers (or basic extractants). Class A forms a small number of almost purely covalent inorganic compounds that are extracted by nonsolvating organic solvents. Class B are formed by neutral coordination-number-saturated complexes between the metal ion and a lipophilic organic acid. Class C is similar to B but makes neutral complexes by acidic ligands and can accept additional uncharged organic molecules, to saturate to coordination sites. If the system does not have any donor molecules (B), the water of hydration may be replaced by undissociated acidic extractants in the organic phase. Class D is ion pair extraction from cation metals that form extractable complexes with large organic anion. Other extractions which are not included in class A, B, C and D are considered as class E.

1. 3.   Reverse micelles in solvent extraction system: improving extraction vs. forming third phase

Recently, reversed micellar extraction has been studied over a wide range of fields because of its thermodynamic stability. A reverse micelle may be formed by a surface-active agent which consists of a long aliphatic part and a hydrophilic group, usually in the opposite end of the molecule compared to the aliphatic chains. These surfactant molecules

are arranged with the polar part in the inner side of the reverse micelle which can encapsulate a nanoscopic water core while the aliphatic parts face outward and are dispersed in the organic solvent. If the surfactant is ionic and contains a single hydrocarbon such as sodium dodecyl sulphate (SDS), reverse micelles are only formed if a co-surfactant (e.g., a medium size aliphatic alcohol) and electrolyte (e.g., 0.2 M NaCl) are added to the system. However, a co-surfactant is not necessary for double chain ionic surfactants such as AOT.

Osseo Asare[16] pointed out that similarities exist between the behavior of "surfactants" and those of "extractants". Based on these studies, the presence of aggregates in the TBP solution used in the PUREX process was expected and observed. Indeed, due to their suface-active properties, extractants are able to self-organize in regular and reverse micelles, although with lower free energies of micellization and therefore lower aggregation numbers compared to surfactants. Following this supramolecular or colloidal scale dominated by interactions weaker than covalent bonding, studies in the literature reported on the aggregation of various extractants in non-polar diluents. Using vapor pressure osmometry[17-19], nuclear magnetic resonance[20], or small angle scattering[21-23], it is possible to investigate the stoichiometry and the aggregation of the complexes formed in the organic phase.

Studies of the solvent extraction of lanthanides and actinides are generally performed under the ideal conditions of low concentrations of cations and extractants, that generally promote the biphasic extraction. In this condition, targeted metal ions are extracted as metal-extractant complex or as metal ions in the core of a reverse micelle. However, the extractant concentration is generally high and the organic phase often

approaches saturation with respect to the extracted species under the conditions met in practice. Under more realistic conditions, this single reverse micelle including an extracted metal ion can form bigger aggregates through the intermicellar attraction which take place between the polar cores of the reverse micelles resulting in a third phase[24]. To understand the extraction mechanism under these conditions, experimental approaches that combine the concepts of coordination chemistry and colloid chemistry have been useful. This can aid in the understanding of the chemical species and energetic driving forces responsible for a variety of phenomena including the formation of the third phase.

1.4   Characteristics of Lanthanides and Actinides

All but one of the lanthanides are f-block elements, corresponding to the filling of the 4f electron shell. Lanthanides exhibit a number of features in their chemistry that differentiate them from the d-block metals. They have a very wide range of coordination number generally from 6 to 12 and their geometries are determined by ligand steric factors rather than crystal field effect. They form labile ionic complexes that may go through exchange of ligands. They have small crystal-field splitting and exhibit very sharp electronic spectra in comparison with the d-block metals[25]. They prefer anionic ligands with donor atoms of rather high electronegativity such as O and F. Furthermore, they can easily form hydrated complexes on account of the high hydration energy of the small Ln^{3+} ion, which can cause uncertainty in assigning coordination numbers. They do not form $Ln=O$ or $Ln\equiv N$ multiple bonds of the type known for many transition metals and certain actinides. Unlike the transition metals, they do not form stable carbonyls and have no chemistry in the 0 oxidation state[26].

The pattern of oxidation state of the early actinides resembles those of d-block metals with the maximum oxidation state corresponding to the number of 'outer shell' electrons. Thus, the chemistry of thorium is essentially confined to the +4 state while uranium exhibits oxidation state of +3, +4, +5, and +6. Ubiquitous to the mid actinides (U, Np, Pu, Am) is rich redox chemistry where oxidation states of +3, +4, +5 and +6 are accessible through standard chemical techniques. More notable, the oxidation states of +5 and +6 of these elements are characterized by a linear dioxo actinyl cation O=An=O. This structural feature is unique to these mid actinides and provides them stark chemical differences from the rest of the actinide series as well as from the lanthanide elements. The linear actinyl moiety of the mid actinides affords unique binding characteristics for complexation and extracting compounds taking advantage of the steric demands of the moiety in a separation process. The differences in oxidation state stability of the actinides are exploited and provide a means for partitioning in separation processes[27-28].

1.5 UV-Vis spectroscopic studies of lanthanide complex

4f electrons of lanthanides yield two types of transitions such as f-f and f-d transitions. The f-f transitions give rise to sharp, narrow bands of comparatively weak intensities which are from Laporte forbidden transition, whereas allowed f-d transitions are relatively broad and intense[29]. Their intra-4f electronic transition, the so-called f-f transition, is one of the most discriminative properties and used extensively for many optics applications such as laser, fibers, optical displays, and biosensors. Because of their sensitivity, this f-f transition is called hypersensitive transition and it is characterized by variations in the intensity of absorption bands in different media. This transition is affected

by the environment of the lanthanides and there are several factors that affect the hypersensitive peak:

1) The intensity of the hypersensitive band is related to the symmetry of lanthanide ion. Especially when polarizable ligands with high symmetry are applied in the system. The field gradient disappears and the magnitude of the induced f → f transition is insignificant and show low intensity. Simply put, the intensity decreases with increasing symmetry[30].

2) Increasing polarity of the ligand binding to the lanthanide increases the intensity of the f → f transition band because the electron donating ability of the ligand influences the f → f transition in the same direction which is affected by the polarizing power (z/rz^+) of the surrounding cation in the second coordination sphere of the lanthanide ion[31].

3) The absorption peak shape changes with different coordination number because of the possible distortion caused by the nearest neighbor cation. Also, hydrated water bound to lanthanide ions from the different media solution affect the spectral change[32].

Table 1.2 Hypersensitive transitions in lanthanide spectra [32]

Lanthanide	Transitions	Wavelength / nm
Praseodymium	$^3H_4 \rightarrow {}^3P_1$	473
Neodymium	$^4I_{9/2} \rightarrow {}^4G_{6/2}, {}^2G_{7/2}$	567-590
Samarium	$^6H_{5/2} \rightarrow {}^6P_{3/2}$	390, 410
Europium	$^7F_0 \rightarrow {}^5D_2$	465
Dysprosium	$^6H_{15/2} \rightarrow {}^6H_{9/2}$	1300
Holmium	$^5I_8 \rightarrow {}^5G_6$	450
Erbium	$^4I_{15/2} \rightarrow {}^2H_{11/2}$	525
Thulium	$^3H_6 \rightarrow {}^3F_2$	790

1.6 Small Angle X-ray Scattering (SAXS)

Small Angle x-ray scattering is sensitive to the electron density difference between core and hydrocarbon corona of reverse micelles and thus this scattering pattern gives the direct information of shape and size of the aggregates. To obtain the meaningful information from the scattering pattern, the intensity should be averaged in horizontal angle in Q, the momentum transfer calculated by the following equation,

$$Q = 4\pi \sin\theta / \lambda \qquad (1.2)$$

where 2θ is the scattering angle and λ is the wavelength of the incident X-ray beam.

In general, the total scattering intensity of monodispersed system can be obtained by multiplying particle number density n, structure factor S(q) and from factor P(q).

$$I(q) = nS(q)P(q) \qquad (1.3)$$

For dilute system, the structure factor is close to 1 and I(q) is determined by the form factor which only considers the structure morphology. In this case, the scattering pattern only show a weak scattering pattern that is close to the background[33]. The radius of gyration, R_g is a shape-independent measure of particle size from the root mean square of all the distances in the particle from its center of mass and this can be obtained from the Guinier approximation and the unified fit method conducted with Irena software package[34].

$$\ln I(q) = \ln I(0) - \frac{R_g^2 Q^2}{3} \qquad (1.4)$$

However, the structure factor includes strong oscillation features when the aggregate formation occurs in polydisperse or non-spherical system[33]. The generalized indirect Fourier transform(GIFT) method interprets the SAXS data allowing the simultaneous determination of the form factor and the structure factor from the scattering data and has been successfully used in microemulsion systems[33, 35-36].

The so-called pair-distance distribution function (PDDF), P(r) is important real-space function through GIFT analysis that gives information about size, shape and internal structure of the particle. P(q) is the reciprocal-space function associated with P(r) describing the particle structure. These two functions are connected through the Fourier transform as

$$P(q) = 4\pi \int_0^\infty P(r) \frac{\sin qr}{qr} dr \qquad (1.5)$$

1.7 X-ray Absorption Spectroscopy (XAS)

X-ray absorption spectra are generated by exposing a sample to a beam of X-rays which possess the characteristic energy equivalent to the binding energy for the core electrons of the element of interest. The incoming photon is absorbed and interacts with a core electron of the absorbing element, promoting to unoccupied state (the conduction band) above the Fermi energy propagates away and leave behind a hole[37-38].

While core electrons are excited to the conduction band, distinct features appear before the edge of the spectrum depending on the structure of the absorbing element. This property is shown in the X-ray Absorption Near Edge Spectroscopy (XANES) regime. Which lies approximately 30 eV before and after the absorption edge.   After electrons are promoted to the conduction band, they start to propagate and scatters off of adjacent atoms before returning to fill the core-hole. This is shown as an oscillation in the extended X-ray absorption fine structure (EXAFS) regime. This oscillation can be changed into real radial space through Fourier transform.
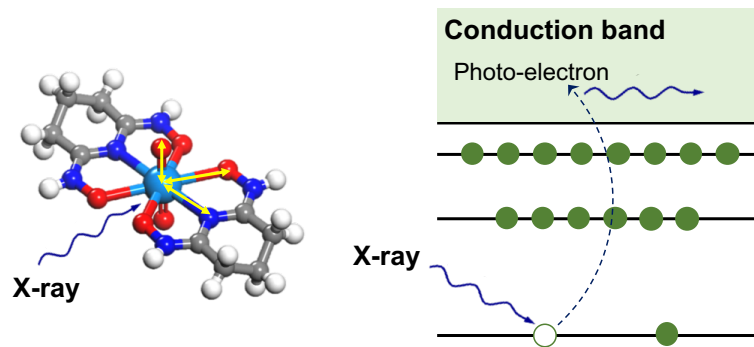
Figure 1.1 The schematic of photoelectric effect, in which an x-ray is absorbed and a core level electron is promoted out of the atom [39]
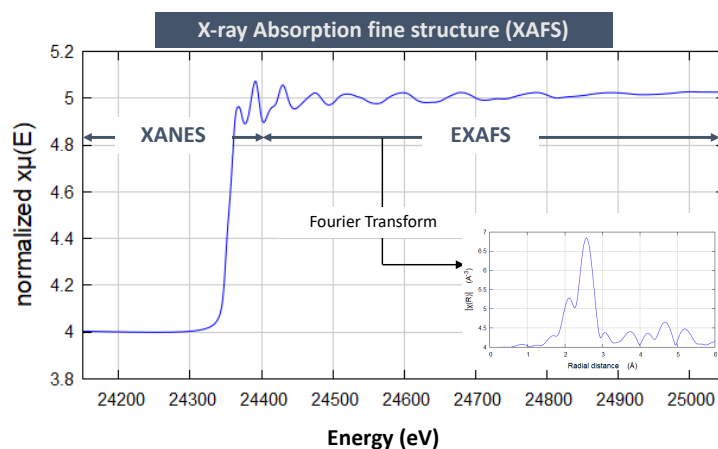
Figure1.2 Overview of X-ray absorption fine structure (XAFS) spectrum

The EXAFS parameter describes the energy-dependent oscillation related to the neighboring atoms via the absorption coefficient μ(E) and can be defined as:

$$\chi(E) = \frac{\mu(E) - \mu_0(E)}{\Delta\mu_0(E_0)} \tag{1.6}$$

The parameter obtained by subtracting off the smooth bare atom background $\mu_0(E)$ and dividing by the edge step $\Delta\mu_0(E_0)$ to give the oscillations normalized to absorption. Since the XAFS is an interference effect between absorbing atom and neighboring atom, it is useful to show the properties in terms of the wave-nature of the photo electron (k) instead of energy term(E).

$$k = \sqrt{\frac{2m(E - E_0)}{\hbar^2}} \tag{1.7}$$

where E_0 is the absorption edge energy and m is the electron mass.

The EXAFS equation[38] becomes

$$\chi(k) = \sum_j \frac{N_j f_j(k) e^{-2k^2\sigma_j^2}}{kR_j^2} \sin\left[2kR_j + \delta(k)\right] \tag{1.8}$$

where R is distance to neighboring atom, N is coordination number of neighboring atom, σ^2 is mean-square disorder of neighbor distance and f(k) and δ(k) are photo-electron

scattering properties of the neighboring atom. The scattering amplitude f(k) and phase-shift δ(k) are changed with atomic number Z of the scattering atom and thus the species of the neighboring atom can be determined by EXAFS equation.

1.8 Scope of Thesis

The overall goal of this research is to elucidate the mechanism of synergistic extraction of mixed extractants system including surfactant and neutral extractant. To accomplish this, we investigated the system with a multistep approach as follows:

1. Identify the extraction mechanism of surfactant (Aerosol OT) itself from aqueous phases containing different acid concentration and ionic strength. The physicochemical properties including water contents and conductivity test and UV-Vis spectra were provided to elucidate the reverse micellar extraction mechanism of lanthanide. This will be discussed in greater detail in chapter 2.

2. Investigate the coordination chemistry aspect in the organic phase upon extraction with AOT : CMPO through use of UV-Vis-NIR and X-ray absorption spectroscopy to determine the mechanism of synergistic effect This will be described in greater detail in chapter 3.

3. Investigate the macromolecular behavior of the organic phase with the use of small angle X-ray scattering to characterize an improved understanding of the extractant metal structure in addition to coordination chemistry, as described in chapter 4.

CHAPTER 2: INFLUENCE OF IONIC MEDIUM ON EXTRACTION OF LANTHANIDES BY AOT REVERSE MICELLES

The work described in this chapter aims to investigate the properties of reverse micelles formed during the extraction of holmium using AOT under different conditions that affect the stability and extractability. Also, we report here results from a small angle X-ray scattering (SAXS) study on AOT/water/heptane performed as a function of the AOT concentration to investigate the effect of varying concentration of the surfactant. SAXS is sensitive to the electron density difference between the core and the surrounding hydrocarbon corona of reverse micelles so that the scattering pattern provides a direct evidence into the shape of the aggregates. We used the generalized indirect Fourier transformation (GIFT) method[40] to analyze the SAXS data and to provide the size and shape information of the reverse micelles formed from AOT.

2.1 Experimental Method

Aqueous solutions of 1×10^{-4} M and 1×10^{-2} M of holmium were prepared by first dissolving holmium oxide (99.999%) provided by Michigan Metals & Manufacturing, in nitric acid to prepare a stock holmium nitrate solution that could then be diluted to appropriate concentration. Concentrated nitric acid (15.8 M) was supplied by Marcon Fine Chemicals. Water used to dilute concentrated solutions was obtained from an in-house source of ultrapure (18.2 MΩcm) water. Sodium nitrate was obtained from Fischer Scientific and was filtered and recrystallized before use. Sodium docusate (AOT) anhydrous

was obtained from Fisher Scientific to >99 % purity. Organic solutions containing different concentration of AOT were prepared by dissolving AOT in heptane (HPLC grade, >99.0 %) obtained from OmniSolv. The organic chemicals were all used without any further purification.

Aqueous solutions for the extraction experiments were prepared by diluting the holmium stock solution to appropriate concentration in nitric acid. These solutions were subsequently standardized for Ho^{3+} concentrations, acidity (H^+ concentration) and excess nitrate concentration by a combination of neutron activation analysis, potentiometric titration, and ion chromatography. Solvent extraction experiments using varying concentrations of AOT in heptane were performed by contacting equal volumes of the organic and aqueous phase for 10 min using a vortex mixer followed by centrifugation at 3000 rpm for 3 min. After centrifugation, aliquots of each phase were taken for analysis. The distribution ratios of Ho (D, defined as the ratio of total Ho concentration in organic over aqueous phase) were determined by neutron activation analysis using the UC Irvine TRIGA® reactor. The holmium was activated to produce [166]Ho and the activated samples were analyzed using a High Purity Germanium (HPGe) detector (30% relative efficiency, Canberra). UV-vis spectra of the organic phases were collected on an Olis upgraded Cary 14 UV-vis-NIR spectrometer with a jacketed cell held at 20°C. The organic phase spectra were collected after extraction with different extractant concentrations. The water concentration in the organic phase was determined with Karl Fisher titrations using a Metrohm KF Titrando with each sample measured in duplicate. The Karl-Fisher measurements were checked for accuracy using standardized solutions of 1 mg water per 1 g solution, HYDRANAL® Water Standard 1.0 obtained from Fisher Scientific.

The electrical conductivity of stirred AOT solutions prepared by sequential dilution of a solution concentrated in AOT were measured with a conductivity meter with a 4-electrode conductivity cell (cell constant of 0.475 cm^{-1}) from Thermo Scientific™ Orion™ DuraProbe™. The cell was calibrated with KCl standard solutions of known conductivity before the measurements. Titrations were carried out using concentrated AOT solutions prepared in both water and heptane to see the solvent effect. Each solution was titrated into a 1x10^{-4} M holmium solution to measure the conductivity change of the initial holmium solution. The critical micelle concentration (cmc) was evaluated from a plot of the conductivity against the surfactant concentration. During the titration, the solutions were equilibrated after each volume addition until a stable conductivity value was obtained. SAXS was performed at the Advanced Photon Source (Argonne National Laboratory) at beamline 12-ID-C with a monochromated incident X-ray beam of 18 keV providing good X-ray transmittance for all solution systems. Samples were contained in 2 mm diameter quartz capillary tubes (Charles Supper Co., 20-QZ). The sample-to-detector distance was adjusted to provide a detecting range for momentum transfer of $0.02 \leq q \leq 1.2$ Å^{-1}, where q was calibrated using a silver behenate standard. Background subtraction of the heptane solvent and the capillary was performed with a single capillary tube for each sample to obtain data without capillary-to-capillary variation. The final scattering curve was obtained from the subtraction of the capillary and solvent.

2.2 Result and Discussion

To establish the behavior of AOT in the liquid-liquid extraction system, extraction experiments were conducted with varying concentration of AOT in heptane in contact with

an aqueous phase with different holmium concentration consisting of either 1×10^{-4} M or 1×10^{-2} M of holmium.

For the experiments with low holmium concentration poor extractability was observed (D < 0.5) and different types of emulsion was formed with increasing concentration of AOT, see Figure 2.1. Emulsification of AOT is caused by the special properties of AOT where the double chain structure provides enough lipophilic character to make an emulsion without the addition of a co-surfactant. Also, flocculation, which is the process whereby the particles of the dispersion form larger-size clusters, can occur in AOT systems under vigorous mixing[41]. As the AOT concentration increased the organic phase became cloudy and increased in volume relative to the aqueous phase. As AOT concentration increases further the system appear to undergo phase transition into a single microemulsion phase and at even higher AOT concentration the organic phase becomes clear and a denser, cloudy phase appear as a third phase below the organic phase.

At low ratio of AOT/heptane, the water amount in the organic phase increases linearly with increasing AOT concentration. There is inadequate amount of surfactant to fully saturate the oil-water interface during contact with the aqueous phase and the resulting emulsion is unable to make a separate stable aggregate but instead form links between unsaturated particles (bridging flocculation) in the organic phase. As the concentration of AOT increase, excess AOT in the form of small aggregates may dissolve in the aqueous phase and form micelles. When the dispersed emulsion droplets approach each other to within a distance that is smaller than the size of the micelles, exclusion of micelles takes place. This forms a micelle-free zone in the organic phase and cause the

drastic decrease of water content in the organic phase[42]. These phase transitions are also observed in the formation of the different emulsions described above.
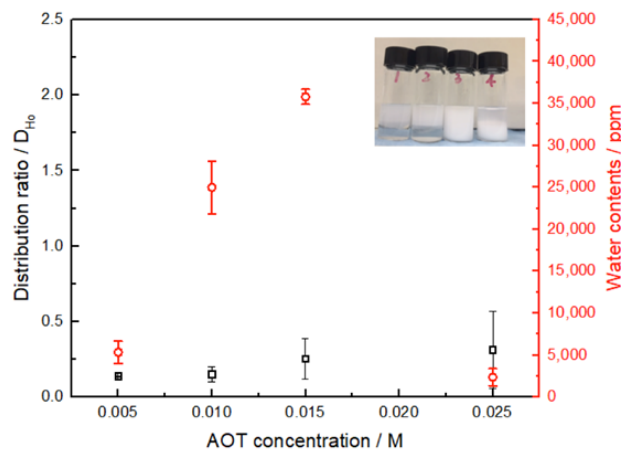
Figure 2.1 Distribution ratio for 1×10^{-4} M Ho^{3+} as a function of AOT concentration. The error bars represent one standard deviation based on triplicate measurements. The insert photo on the top right shows visual appearance of solution after contact with different concentration of AOT in the heptane (Vial #1: 0.010 M, Vial #2: 0.015 M, Vial #3: 0.020 M and Vial #4: 0.025 M AOT). The distribution ratio and water content in the organic phase for the case of 0.020 M AOT is missing due to its single-phase emulsion state.

In previous work from our lab[43], we successfully utilized conductivity as a probe for the surfactant behavior and showed that it was useful in predicting the microstructure of the liquid phases and can be coupled to metal extraction. Conductivity measurements has been widely used to obtain the critical micelle concentration (cmc) of ionic surfactants[44] and generally, the cmc or cvc (critical vesicle concentration) is determined by discontinuity in the slope of the conductivity as a function of the surfactant concentration. Here, to

further investigate the properties of AOT, conductivity measurements were carried out in the presence of holmium.

Figure 2.2 (a) shows the conductivity measurement by titrating with AOT aqueous and organic solution into a solution of 1×10^{-4} M holmium. The change of the slope in the conductivity-versus-concentration plot demonstrates the formation of regular micelles around 0.006 M in the aqueous phase however the solution turned turbid when the concentration was over 0.005 M due to the low solubility of the hydrophobic chain in the aqueous phase. It is interesting to note that our previous studies titrating AOT into an aqueous phase suggested vesicles forming just above 0.006 M[43]. It appears that the presence of holmium, even at low concentration, inhibits the formation of large vesicles. On the other hand, when AOT was added to the organic phase, the cmc value is around 0.002 M which is similar to experiments without holmium. The overall conductivity of the organic solution is lower than the aqueous AOT solution, even though the applied concentration of AOT is the same in both solutions. This can be explained by the differences between the dielectric constants for the aqueous and the organic electrolytes[45].

To examine the formation of reverse micelles and regular micelles, different titration experiments were carried out for the conductivity measurement. A solution of 0.01 M AOT/heptane was titrated into an aqueous solution of 1×10^{-3} M Ho^{3+}. And a solution of 1×10^{-3} M Ho^{3+} was titrated into an organic solution containing 0.01 M or 0.03 M AOT in heptane. Figure 2.2b show the conductivity trends during the titrations. The large variation of conductivity indicates that a phase transition takes place in the region associated with Winsor III or Winsor IV phase behavior which is associated with a three-phase system and

a single-phase micellar solution, respectively[46]. As the aqueous phase is added into the oil

phase, a water-in-oil dispersion results since the water contents is very low and oil drops

can be included in the water drops (o/W/O) which cause a slight increase in the

conductivity in the organic phase. Once this phase reaches the critical point, the internal

emulsion droplets start to coalesce, triggering the phase transition and extensive reverse

micelle formation indicated by the rapid increase in conductivity.
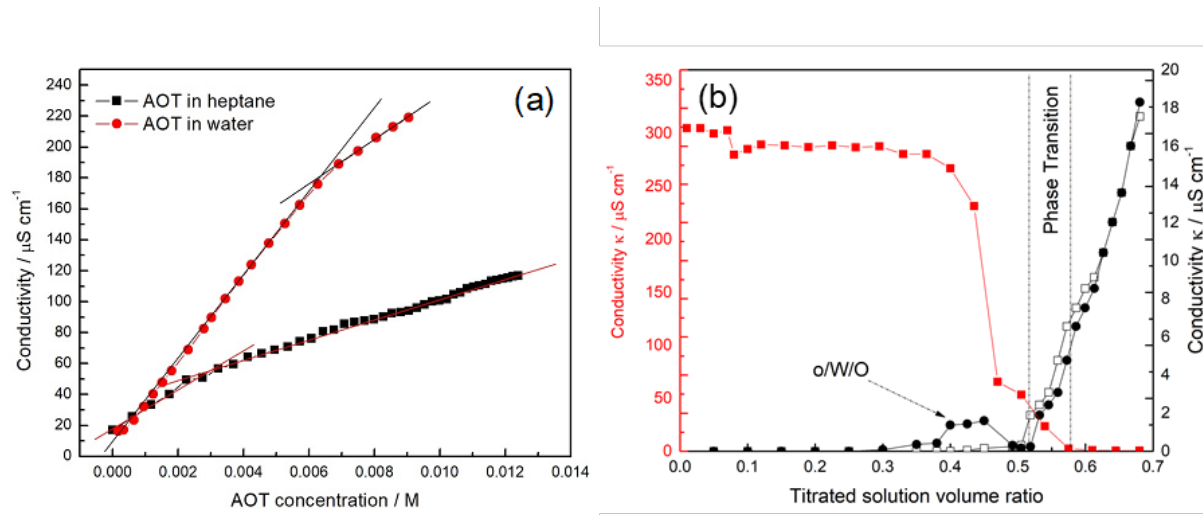
Figure 2.2 (a) Plot of electrical conductivity as a function of AOT concentration. The AOT aqueous solution (red circle) and the AOT organic solution dissolved in heptane (black square) were titrated into the aqueous holmium solution (1×10^{-4} M) (b) Plot of electrical conductivity as a function of water volume ratio. Red symbols show the conductivity change of the aqueous holmium solution (1×10^{-3} M) titrated by 0.01 M AOT/heptane and black symbols show the conductivity change of organic phases (0.01 M AOT/heptane – Black open square, 0.03 M AOT/heptane – Black full circle) titrated by holmium aqueous phase solution (1×10^{-3} M).

Figure 2.3 shows the distribution ratio of holmium with different AOT concentration for

high holmium concentration (1×10^{-2} M) and the measured water contents of the organic

phase as a function of AOT concentration. The distribution ratio and the water content

increase linearly with increasing AOT concentration at high holmium concentration in the

aqueous phase. Also, the flocculation in both the organic and the aqueous phase

disappeared, although there was a small volume of third phase in the interface of the two

phases at high AOT concentration. This third phase can be explained by the excess AOT

absorbed at the interface of two phases. Also, these results matched with other literature

results where water concentration in the non-aqueous phase increase with AOT

concentration[14].
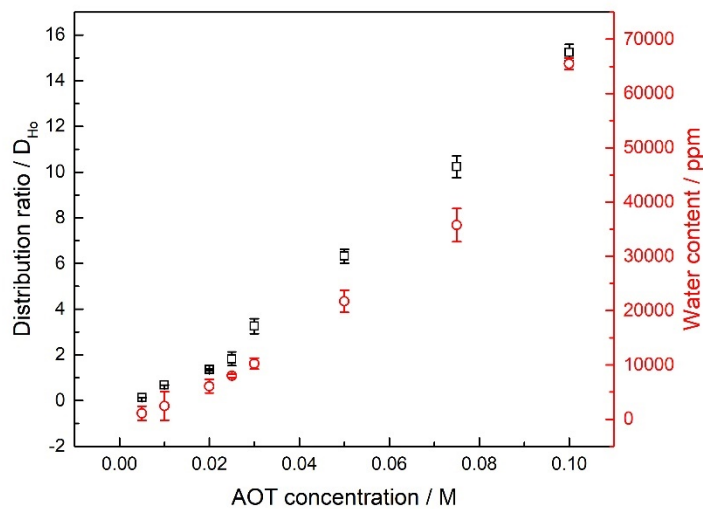
Figure 2.3 Extraction conducted with 1×10^{-2} M Ho(NO$_3$)$_3$ in the aqueous phase with the pH of the initial aqueous phase at 3.5. Distribution ratios of Ho (III) between the aqueous solution and AOT/heptane solution (black square). Water contents of the organic phase after extraction (Red open circle)

To further probe the aggregation phenomena in the organic phase as a function of AOT

concentration, SAXS measurements were performed on solutions before and after contact

with aqueous phases including Ho^{3+} at the higher concentration (1×10^{-2} M). Figure 2.4 shows

the scattering intensity I(q) vs. q obtained from the SAXS experiment with different

concentration of AOT. The scattering contrast for the contacted organic solution is higher than non-contacted solution. Also, every scattering profile is characterized by a shoulder which is attributed to the globular structure of the reverse micelles. The shoulder of the scattering profile from the dry organic phase is located in identical positions for the different AOT concentrations (Figure 2.4 a). For globular systems, such as reverse micelle system, the intensity at I(0) is dependent on the volume(V) of the core of the aggregates according to following equation;

$$I(0) = (\phi V \Delta\rho)^2 P(0)S(0) \qquad (2.1)$$

Here, ϕ is the volume fraction of the scattering aggregates, $\Delta\rho$ is the electron density contrast, and P(0) and S(0) are the form and structure factors, respectively, of the aggregates.
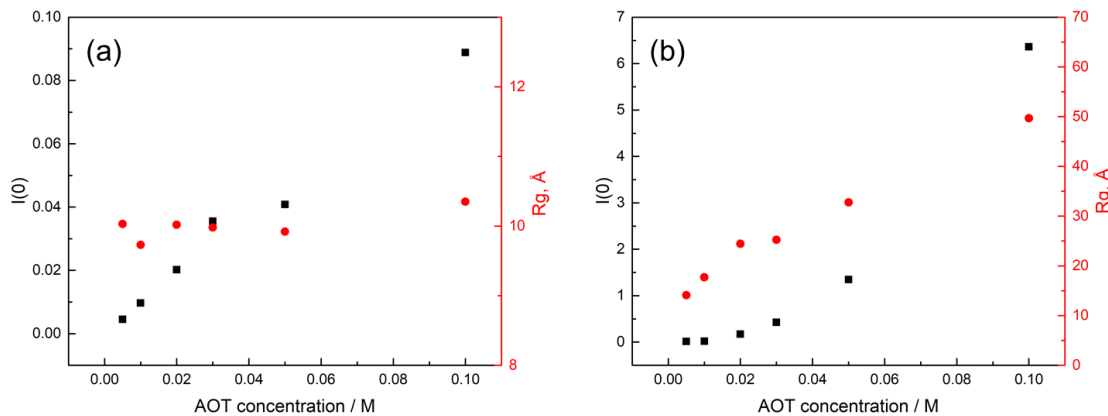
Figure 2.4 I(0) (black) and radius of gyration(Rg, Å) (Red) calculated from the scattering curves (Figure 2.4 (a) and (b)) for the organic phase (a) before contact with the aqueous phase and (b) after contact with the aqueous phase.
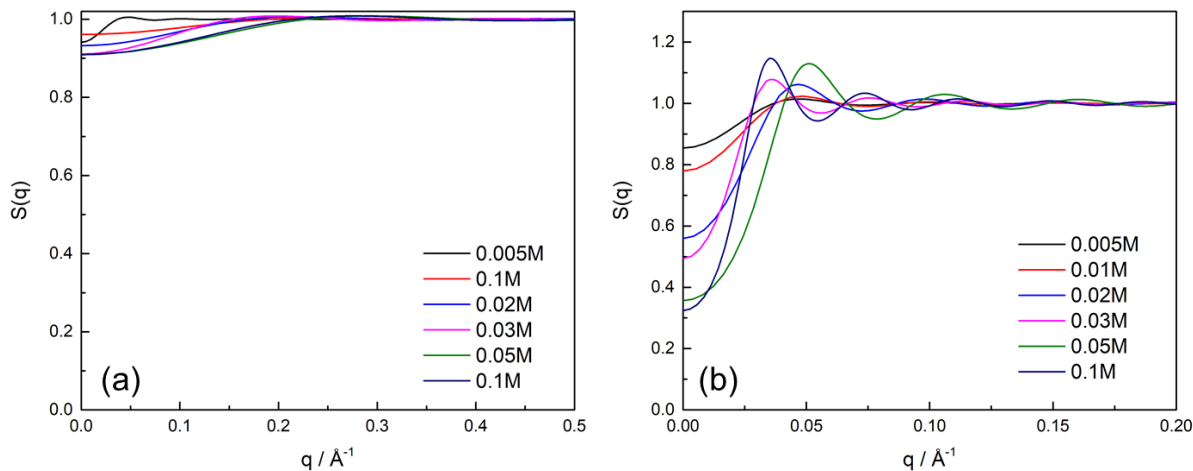
Figure 2.5 Structure factor determined for the organic phase (a) before contact with the aqueous phase and (b) after contact with the aqueous phase

For the organic phase before contact with the aqueous phase, an increasing I(0) trend was observed with increased AOT concentration (Fig 2.4) corresponding to the increase of aggregate volume with AOT concentration. However, the scattering curves show a drastic change for the organic phase which contained extracted Ho^{3+} compared with the organic phase before contact with the aqueous phase. The shoulder around 0.1 $Å^{-1}$ shift to lower q-values and the scattering intensities gradually increases with increasing AOT concentrations. These variations indicate increasing size of the reverse micelle by extracting more water and Ho^{3+} from the aqueous phase with increasing AOT concentration, as well as a possible change in the shape. However, it is hard to draw conclusions based only on the I(0) result due to the high concentration of surfactant and water present. For high concentration samples, the influence of the structure factor results in strong oscillation (Fig2.5), but the I(0) from the Guinier analyses does not take the interaction effects due to the structure factor into consideration[47]. Thus, the pair distance

distribution function (PDDF) result produced by GIFT analysis is important for describing

the aggregates in the organic phase especially for high concentration sample after contact

with the aqueous phase. These results are presented in Figure 2.6.
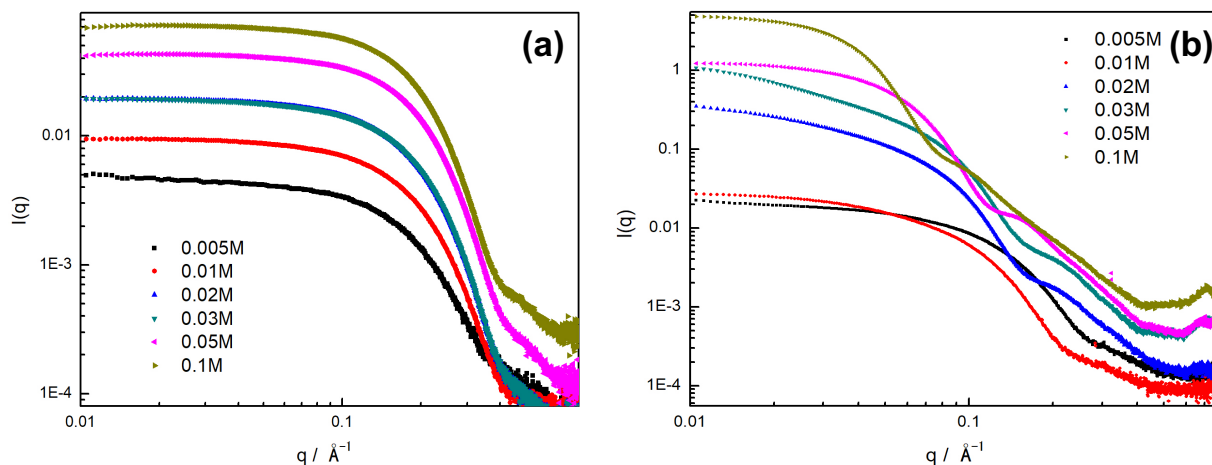
Figure 2.6 Log-log plot of the SAXS data for different AOT concentration (shown in the legend) in heptane. (a) The organic phase before contact and (b) after contact with $1x10^{-2}$ M Ho(NO$_3$)$_3$ in the aqueous phase. Please note the difference in scale between the two graphs.
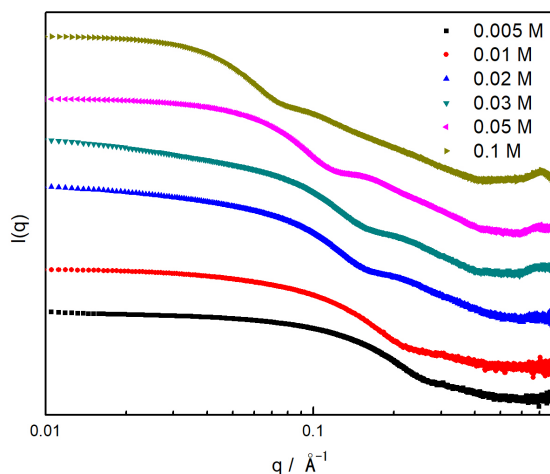
Figure 2.7 Log-log plot of the SAXS data for the organic phase after contact with the aqueous phase. Plots are offset for clarity.

Figure 2.8 shows the profiles of the pair distance distribution function P(r) obtained from GIFT analysis of the scattering profiles in Figure 2.4. For added clarity and easier comparison P(r) plots normalized at the highest peak intensity are shown as well. For the organic phase without metal (Figs. 2.8a and 2.8c), the peak center is located at the same position with increasing AOT concentration and has symmetrical bell-shaped peaks indicating spherical aggregates. However, the organic phase after contact with the aqueous phase that included holmium nitrate (Figs. 2.8b and 2.8d) show different trends. The P(r) function for high AOT concentration shows a relatively symmetrical bell-shaped peak at high concentration of AOT (> 0.03 M), which is typical for a spherical particle with slight shoulder at higher r. However, tailing to large r is observed for the P(r) profiles at concentration of AOT between 0.005 M and 0.03 M, which may suggest minor polydispersity in the dimensions and an elongated shape of the reverse micellar structure. Also, for this AOT concentration range, a low shoulder appears at near double the distance of the bell-shaped main peak position, suggesting a minor presence of reversed micellar oligomers.

In the water/AOT/organic solvent system, this behavior can be explained by transition from a metastable oligomeric phase to a monomeric phase of reverse micelle with different water-to surfactant ratio (w_0 = [H_2O]/[AOT])[48,49]. Water-to-surfactant ratio is one of the important factors that affect the size of the reverse micelle in a water/AOT/organic solvent system and it is known that the transient oligomerization of reverse micelles occurs at $10 < w_0 < 25$[48]. As shown in Figure 2.9a, the corresponding water-to-surfactant ratio of the tailing graphs exists in the oligomerization transition range which correspond with the literature range cited above.
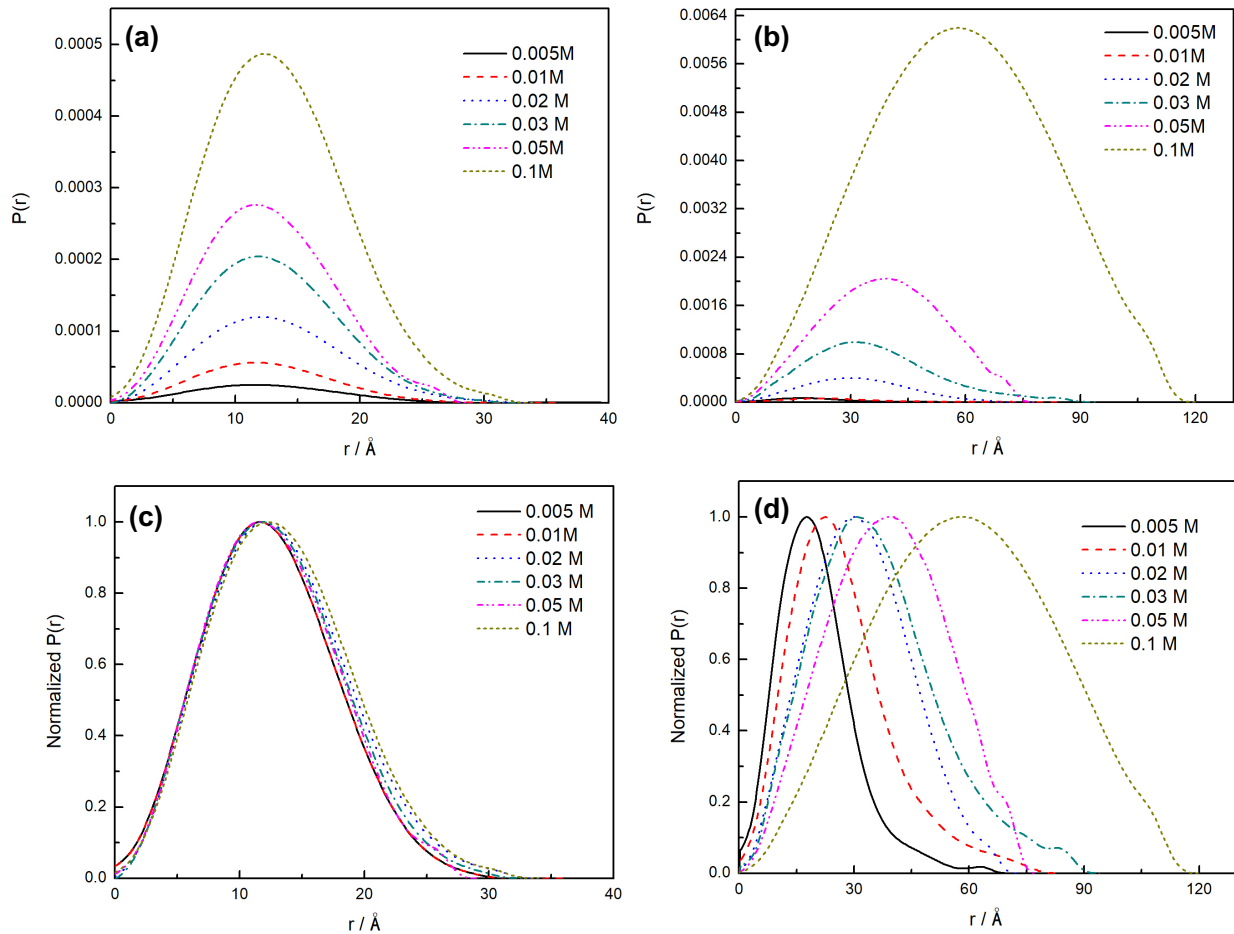
Figure 2.8 Variation of the pair distance distribution function P(r) of the organic phase with different AOT concentration after contact with the aqueous phase with 1×10^{-2} M holmium (III) nitrate. The P(r) function is calculated from the scattering profiles in Figure 2.4. (a) shows the P(r) profiles for the organic phases with the different AOT concentration before and (b) after contact with the holmium containing aqueous phase. Normalized P(r) of (a) and (b) is also showed in (c) and (d) respectively.

To determine the trend of droplet size and shape with different AOT concentration, the highest intensity peak position, r_{Pmax} values are plotted in Figure 2.9 (b) as a function of water-to-surfactant ratio. The plot shows good linearity and has a slope of 1.5 in the whole w_0 range, suggesting the change of the reverse micelle radius was caused by the linear uptake of water.
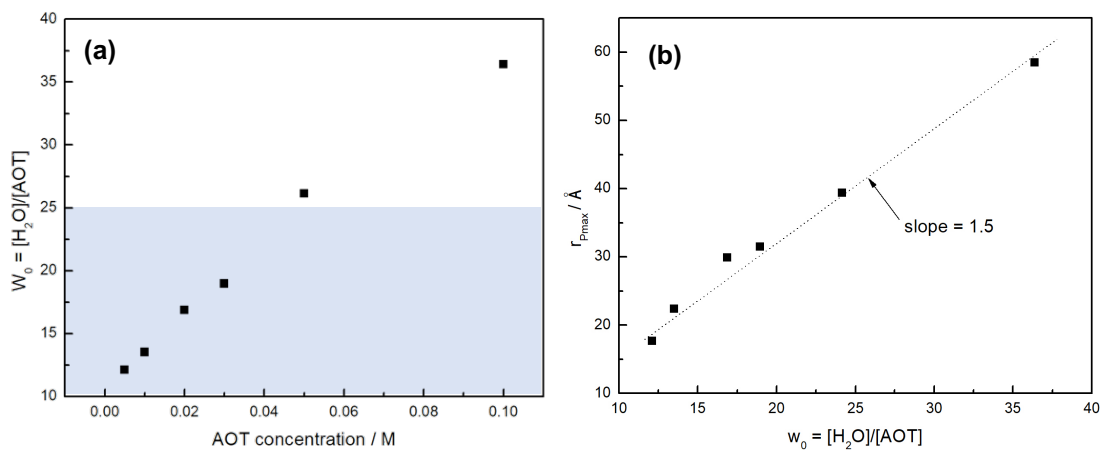
Figure 2.9 (a) Plot of the analyzed water-to-surfactant ratio as a function of the AOT concentration, corresponding with the data in Figure 2.4b. The region where oligomerization is expected to occur based on the water to surfactant ratio is shown with a blue shade. (b) Plot of the r value corresponding to the peak position P_{max} as a function of the water-to-surfactant ratio w_0. Each point of the graph was obtained from Figure 2.5b.

In the same way of increasing metal concentration, ionic strength is an essential variable for controlling the size of both regular micelles and reverse micelles. It has been shown that the salt cause a decrease in the size of reverse micelle since the electrical double layer becomes thinner[50]. The effect of ionic strength on the microemulsion formed by AOT is not well studied in the respect of metal extraction. In addition to ionic strength, the pH in the aqueous solution which the holmium is dissolved in is also of importance in the extraction system by AOT due to the deformation of the AOT molecule, discussed below. To investigate the effect of ionic strength and pH on the AOT extraction system, the organic phase including 0.01 M of AOT was contacted with aqueous solutions of different concentration of HNO_3 and $NaNO_3$ including 1×10^{-2} M Ho^{3+}.
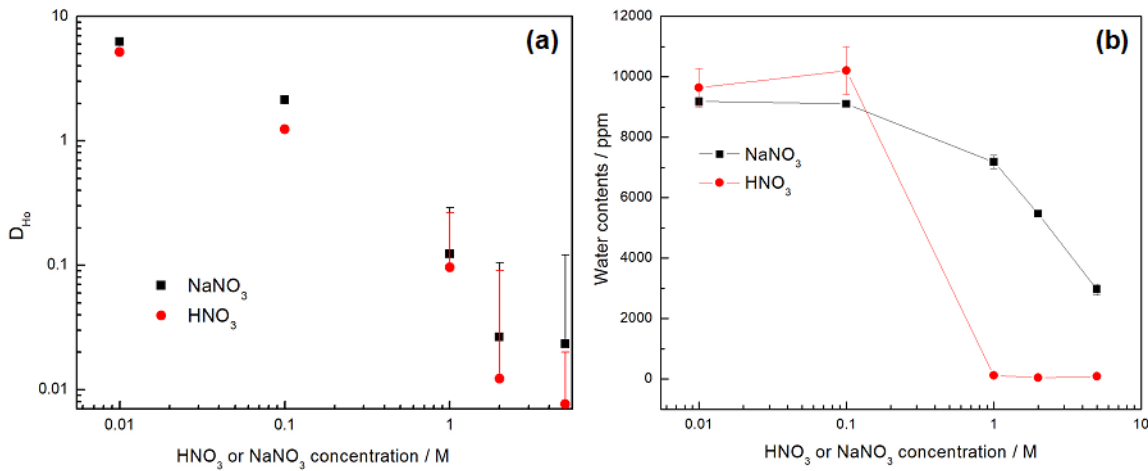
Figure 2.10 Extraction conducted with 1×10^{-2} M $Ho(NO_3)_3$ dissolved in different concentration of HNO_3 and $NaNO_3$ using 0.05 M AOT in heptane. (a) Distribution ratio of Ho(III) (b) Water content in the organic phase after extraction.

Figure 2.10 shows the distribution ratio of holmium and the water content in the organic phase as a function of the concentration of $NaNO_3$ and HNO_3 in aqueous phase. In both HNO_3 and $NaNO_3$ aqueous solutions, it is seen that the distribution ratios of holmium decrease with increasing concentration of HNO_3 and $NaNO_3$. The water content is gradually decreased from 9000 ppm to 2000 ppm with increasing concentration of $NaNO_3$. On the other hand, the water concentration completely drops to 0 at higher HNO_3 concentration which indicates that AOT can no longer form reverse micelles. This can be explained by the deformation of AOT from sulfonate to sulfonic acid (Figure 2.11). According to Suzuki et al.[51], the H^+ ion has a negative effect on the microemulsion because it promotes the formation of sulfonic acid by substituting the Na^+ ion with a H^+ ion.

R1=ethyl, R2=butyl
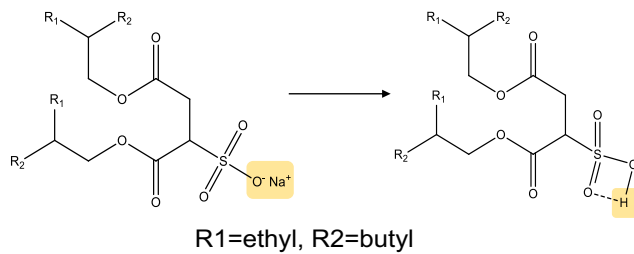
Figure 2.11 The deformation of AOT after equilibrated with an aqueous HNO_3 solution.

Additional amounts of Na^+, on the other hand, does not show any gradual decomposition of the W/O microemulsion nor any deterioration of the AOT anion. Both the Ho distribution ratio and water content decrease with the increasing concentration of $NaNO_3$, which suggests holmium extraction follows a cation exchange mechanism and that the proton as well as sodium competes with holmium for coordinating with the AOT sulfonate group.

Figure 2.12 shows the UV-Vis spectra of the organic phase after contact with HNO_3 and $NaNO_3$ aqueous phases including holmium nitrate. The peaks at 279 and 284 nm show the extracted holmium in the organic phase and the broad band centered around 300 nm correspond to nitrate. At low concentrations of HNO_3 or $NaNO_3$, holmium absorption bands are present while the nitrate band did not appear. The features of the holmium spectra disappear and the intensity of the nitrate band in the organic phase increase at higher nitric acid and nitrate concentration suggesting a competition in the uptake, as seen in figure 2.10a. In the case of nitric acid, it shows higher nitrate absorbance compared to sodium nitrate. From these results, we can ascertain that high acidity results in the sulfonic acid deformation of AOT causing it to not be able to make reverse micelles but still allows the

31

uptake of the nitrate from the aqueous phase possibly as the HNO$_3$ molecule. For aqueous phases including NaNO$_3$, the nitrate extracted into the organic phase is likely incorporated in the reverse micelle since the deformation of AOT does not occur and there is extensive water uptake into the organic phase.
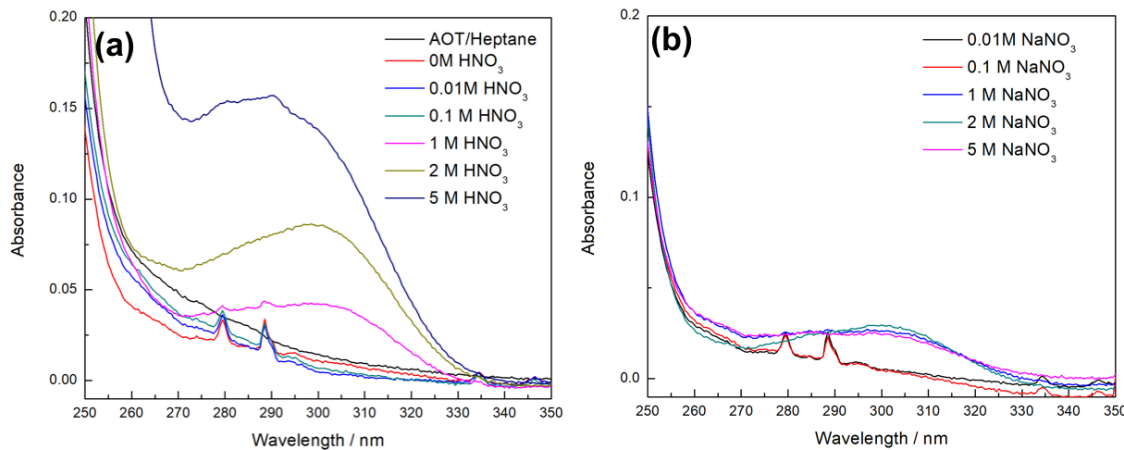
Figure 2.12 UV-vis spectra of organic phase after contact with (a) different concentration of HNO$_3$ and (b) different concentration of NaNO$_3$ in aqueous phase. The extraction conducted with 1×10^{-2} M Ho(NO$_3$)$_3$ initially in the aqueous phase and 1×10^{-4} M AOT in heptane as the organic phase.

2.3 Conclusion

We observed the extractability and stability of Aerosol OT in the extraction system drastically improved with increasing target metal concentration in the aqueous phase. At low concentration of holmium in the aqueous phase, the flocculation was dominant but for high metal concentration in the aqueous phase, the flocculation did not occur and the organic phase showed good extractability.

SAXS data were collected for organic phases both before and after extraction to analyze the change of size and structure of reverse micelle with different AOT concentration from 0.005 M to 0.1 M. We could verify that the AOT reversed micellar structure change with varying AOT concentration and water-surfactant molar ratio, w_0. According to the P(r) function analysis the organic phases, before contact with an aqueous phase, showed same location of P_{max}, which corresponds to the radius of the reverse micelle. However, a significant increase was observed for the radius with increasing AOT concentration after the organic phase was contacted with the aqueous phase containing holmium. We correlated the P_{max} with the water-surfactant molar ratio and showed that there is a great likelihood of a metastable oligomeric phase at low w_0 region ($w_0 < 25$).

The ionic strength and pH of the aqueous phase was shown to affect the metal uptake of AOT as the metal ion is extracted by an ion exchange mechanism. The AOT reverse micelles were shown to not be stable at high acidity due to the deformation of the molecule as it converts from sulfonate to sulfuric acid. The deformed AOT extract nitrate from the aqueous phase in place of Ho^{3+}.

Overall, these results provide insight into the role of AOT as an extractant for lanthanides although its use by itself is limited. The results and conclusions presented here will be of value for future studies of synergistic systems using AOT in combination with other, more established, extracting reagents.

CHAPTER 3. COORDINATION CHEMISTRY OF LANTHANIDES IN AOT-CMPO SOLVENT EXTRACTION SYSTEMS; UV-Vis AND XAFS STUDIES

In this chapter, I investigate how a combination of AOT and a neutral extractant in an extraction system for metal ions affects the solute extractability and the phase stability with respect to coordination chemistry. Holmium (Ho) and erbium (Er) were chosen as a target metals due to their spectroscopic properties that include hypersensitive bands responsive to the coordination and geometry of surroundings. Water, metal ion and nitric acid extraction were carefully monitored as a function of AOT to neutral extractant concentration ratio. The complexation state of extracted species with AOT and CMPO was investigated by spectroscopic analyses such as UV-Vis spectroscopy[32, 52-53] and X-ray Absorption Spectroscopy (XAS).

For certain lanthanides, the electron transitions are hypersensitive to the symmetry and electronic field strength of the metal such as $^5I_8 \rightarrow {}^5G_6$ transition for Ho and $^4I_{15/2} \rightarrow {}^2H_{12/2}$ transition for Er[32]. Since the mechanism of each extractant, AOT and CMPO, are different, the electron transition of the extracted lanthanide will help to understand if and how the lanthanide environment changes during the extraction. In addition to the UV-Vis study, we applied X-ray Absorption spectroscopy (XAS) as a technique to better understand the coordination chemistry around the metal ion. The Fourier transform of extended X-ray absorption fine structure (EXAFS) enables a first qualitative estimate of how many atoms are present in each coordination shells at certain distances surrounding the absorbing atom. This is done by analyzing the spectrum in either k or R space through Fourier

transform. In addition to XAFS analysis, wavelet-based XAFS analysis is a dedicated method to elucidate the elemental feature and spatial location of the neighbors surrounding the X-ray absorber[54-55]. Especially in solvent extraction system, the extraction conducted with soft donor or mixed donor systems will result in complexes which has similar bond length between the targeted metal ion and the different donor groups. To better understand these systems, wavelet transform (WT) of Fourier transform was adapted for discriminating the backscattering atoms by their elemental nature. The WT can resolve the k dependence of the absorption signals and therefore gives better contrast between heavier and lighter backscattering atoms, even if they are at the same distance from the central atom[55-56]. The aim of this work is to investigate the coordination chemistry by means of UV-vis and XAFS to understand the mixed extractant system and the role of each extractant.

3.1 Experimental Method

Aqueous solutions of 0.01 M of holmium and erbium were prepared by first dissolving holmium oxide (99.999%) and erbium oxide (99.999%) provided by Michigan Metals & Manufacturing, in nitric acid to prepare a stock holmium or erbium nitrate solution that could then be diluted to appropriate concentration. These solutions were subsequently standardized for Ho^{3+} and Er^{3+} concentrations, acidity (H^+ concentration), and excess nitrate concentration by a combination of neutron activation analysis, UV-Vis, potentiometric titration, and ion chromatography. Concentrated nitric acid (15.8 M) was supplied by Marcon Fine Chemicals. Water used to dilute the concentrated solutions was obtained from an in-house source of ultrapure (18.2 MΩ·cm) water. Sodium nitrate was obtained from Fischer Scientific and was filtered and recrystallized before use. Sodium

docusate (AOT) anhydrous was obtained from Fisher Scientific to >99% purity. CMPO was obtained at 96% purity from Marshallton. Organic solutions containing different concentration of AOT and CMPO were prepared by dissolving the reagents in heptane (HPLC grade, >99.0%) obtained from OmniSolv. The organic chemicals were all used without any further purification.

Solvent extraction experiments using AOT and CMPO in heptane were performed by contacting equal volumes of the organic and aqueous phase for 5 min using a vortex mixer followed by centrifugation at 3000 rpm for 3 min. After centrifugation, aliquots of each phase were taken for analysis. The distribution ratios of Ho were determined by neutron activation analysis using the UC Irvine TRIGA® reactor. Holmium was activated to produce [166]Ho and the activated samples were analyzed using a High Purity Germanium (HPGe) detector (30% relative efficiency, Canberra). The distribution ratio of erbium was measured by UV-Vis analysis from the difference of the aqueous phase concentration before and after extraction. UV-vis spectra of the organic phases were collected on an Olis upgraded Cary 14 UV-vis-NIR spectrometer with a jacketed cell held at 20°C. The organic phase spectra were collected after extraction with different extractant concentrations. The water concentration in the organic phase was determined by Karl Fisher titrations using a Metrohm KF Titrando with each sample measured in duplicate. The Karl-Fisher measurements were checked for accuracy using standardized solutions of 1 mg water per 1 g solution, HYDRANAL® Water Standard 1.0 obtained from Fisher Scientific.

XAFS investigations were performed at beamline 10-BM-B of the Advanced Photon Source at Argonne National Laboratory[57]. Spectra were collected at the holmium L-III edge (8071 eV) and Erbium L-III edge (8358 eV) in fluorescence mode with a Hitachi Vortex-

ME4 four element silicon drift fluorescence detector. For all samples, data sets were collected until adequate signal to noise was obtained, in all instances between 3 to 10 scans. The X-ray white beam was monochromatized by a Si (1 1 1) monochromator and detuned 50% to reduce the contribution of higher-order harmonics. All samples were collected at room temperature.

Data were processed with the Athena and Artemis programs of the IFEFFIT package[58]. Spectra were averaged in $\mu(E)$ data, which was calibrated to the literature E_0 value for each elements edge. Background removal was achieved by spline fitting. EXAFS data were extracted above the threshold energy, E_0. The conventional metrical analysis of the Ho and Er $k^3\chi(k)$ EXAFS was performed. Fit windows in k space were determined based on the lowest quality data collected and for all data sets were from 1 to 9 Å^{-1}. In all fits, the amplitude reduction factor (S02) was performed with a fixed scale factor as 0.9. Independent structural parameters determined by the fits included the change in the scattering half path length (ΔR_i) and the relative mean square displacement of the scattering element (σ_i^2). For each fit, the number of variables was not permitted to exceed 2/3 the number of independent points, in keeping with the Nyquist criterion.

A qualitative analysis of the property of backscattering atoms in higher coordination shells was conducted using the wavelet transform (WT) method implemented in the EvAX code[59]. These WT results are typically visualized as contour plots in three dimensions including the wave vector (k), the interatomic distance uncorrected for phase shift (R) and the WT modulus. Contributions from different back-scattering atoms at specific regions in k and R space are visualized in the plots as ridges and the location of the ridges helps to differentiate between light and heavy backscattering atoms[55].

3.2 Results and discussion

Solvent extraction experiments were performed at varying AOT ratio ([AOT]/([AOT]+[CMPO]) = 1, 0.75, 0.5, 0.25, 0) keeping total extractant concentration (AOT + CMPO) at 0.05 M in the organic phase and contacting with an aqueous phase of different nitric acid concentration with 0.01 M Ho^{3+} or Er^{3+}. Figure 3.1 (a) and (b) shows the variation of distribution ratio of Ho^{3+} and Er^{3+}, defined as the ratio of the concentration of the metal between the organic and aqueous phase. For the extraction from low acid concentrations, an increasing trend for both holmium and erbium is observed although erbium shows lower distribution ratios at high AOT concentration compared to holmium.
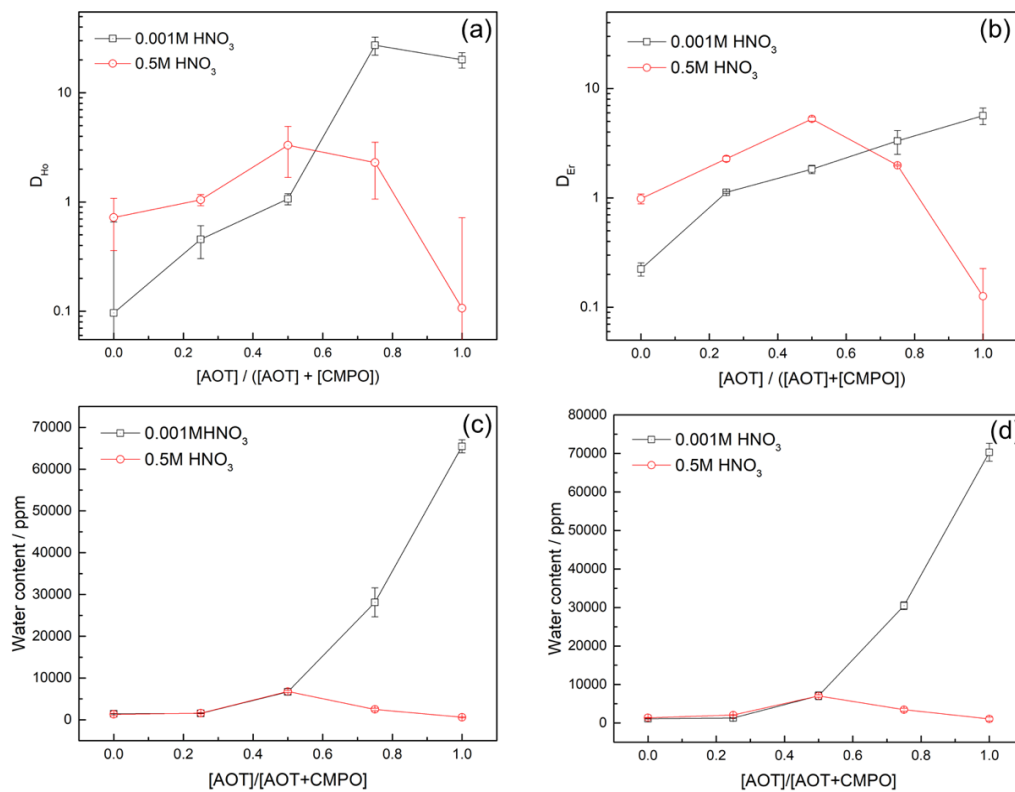
Figure 3.1 Distribution ratio of holmium(a) and erbium (b) and concentration of water in the organic phase (holmium extraction (c), erbium extraction (d)) as a function of [AOT]/[AOT+CMPO] mole ratio after contact with 0.001 M HNO_3 (black) or 0.5 M HNO_3

(red) aqueous phase containing 0.01 M Ho^{3+} or 0.01 M Er^{3+}. The error bars represent standard deviations from triplicate measurement.

When the acid concentration of the aqueous phase increase, a nonlinear trend for both holmium and erbium was observed. At an AOT ratio of 0.5 when the higher acid concentration was used, the distribution ratio of holmium and erbium increased from 0.7 to 2 and from 1 to 4, respectively. This suggest that the cooperative effect of CMPO is possibly due to the increase of extractability of CMPO at higher acid concentration. For the experiments at high acid concentration, the distribution ratio drastically decreases at higher AOT concentrations, which can be explained by the deformation of AOT at higher acid concentration[51] and the concentration of CMPO not being enough to extract additional lanthanides from the aqueous phase. The fact that the distribution ratios, in the high acid case, for an AOT ratio of 0 is lower compared to the AOT ratio of 0.5 suggest that there is a synergistic effect. If there was no synergistic effect the solvent using 0.05 M CMPO alone should provide the highest extraction at high acid.

In addition to the distribution ratio, the water content of the organic phase at each AOT ratio was analyzed and is shown in figure 3.1 (c), (d). A linear trend for Ho^{3+} and Er^{3+} were observed for low acid concentration, but a non-linear trend is observed for the high acid concentration. While the water content trend is similar to the trend of the metal distribution ratio at high nitric acid concentration, the differences in water content between high and low acid case at the AOT ratios of 0.25 and 0.5 were very small. This suggests that the amount of reverse micelle formed is similar between low and high acid concentration, at these AOT ratios. Due to the amphiphilic property of AOT, it can dissolve in both the aqueous and the organic phase and cause a phase change from micelle to

emulsion phase if enough water is extracted into the organic phase. From our previous study[43], the emulsion phase of the organic phase occurred at lower AOT concentration, less than 0.02 M AOT, but the emulsion in the aqueous phase formed when AOT was added in a concentration above 0.02 M. However, this phenomenon did not occur for the mixed AOT-CMPO system and both phases were clear.

UV-vis spectra of organic phases after extraction of metal ions from different aqueous acid concentration were collected at the wavelengths covering the hypersensitive absorption band. The holmium ion has a hypersensitive band centered around 450 nm, related to the $^5I_8 \rightarrow {}^5G_6$ transition. Depending on the coordination number and environment around the lanthanide atom, the peak shape and the intensity change drastically[30, 52].
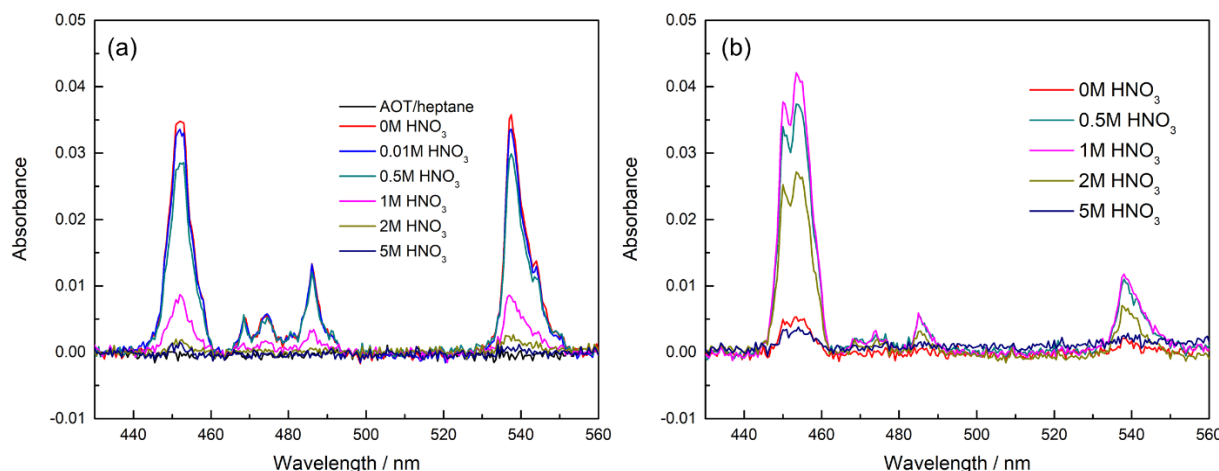
Figure 3.2 UV spectra of organic phases for the acid concentration dependency for holmium extraction with (a) 0.01 M AOT in heptane and (b) 0.01 M CMPO in heptane. Extraction conducted with 0.01 M Ho(NO$_3$)$_3$ dissolved in nitric acid of different concentration.

Before testing the effect of combining AOT and CMPO, the organic phases with the extracted holmium from the experiments using either AOT or CMPO individually were tested. Figure 3.2 shows the organic phase UV spectra after contact using different concentration of nitric acid with AOT (Fig 3.2. (a)) or with CMPO (Fig 3.2. (b)). The data were collected from 430 to 560 nm to see the difference between hypersensitive peak (450 nm) and non-hypersensitivity peak (537 nm). Due to the extractability difference, the intensity of the holmium peak is different between AOT and CMPO extraction. Since the AOT showed higher extractability, the peak intensity of holmium should be higher for the AOT extraction. However, the intensity ratio of the bands centered at 450 nm which correspond to hypersensitive band are similar for both AOT and CMPO extraction and the band centered at 537 nm which correspond to non-hypersensitive transitions are significantly lower for CMPO extraction. This high intensity around 450 nm for CMPO extraction is remarkable, indicating very intense hypersensitive transition compared with the same transition in AOT extraction. This intensity difference can be explained by different symmetrical environment around the extracted lanthanides with different extractant. Our earlier study suggests that AOT extracts lanthanides by forming reverse micelles which includes lanthanide ions solvated by water which can form a symmetrical environment. However, CMPO extracts trivalent metal cation by chelating to the lanthanide and, in addition, the metal ion complex contains NO_3 anions to balance the charge.
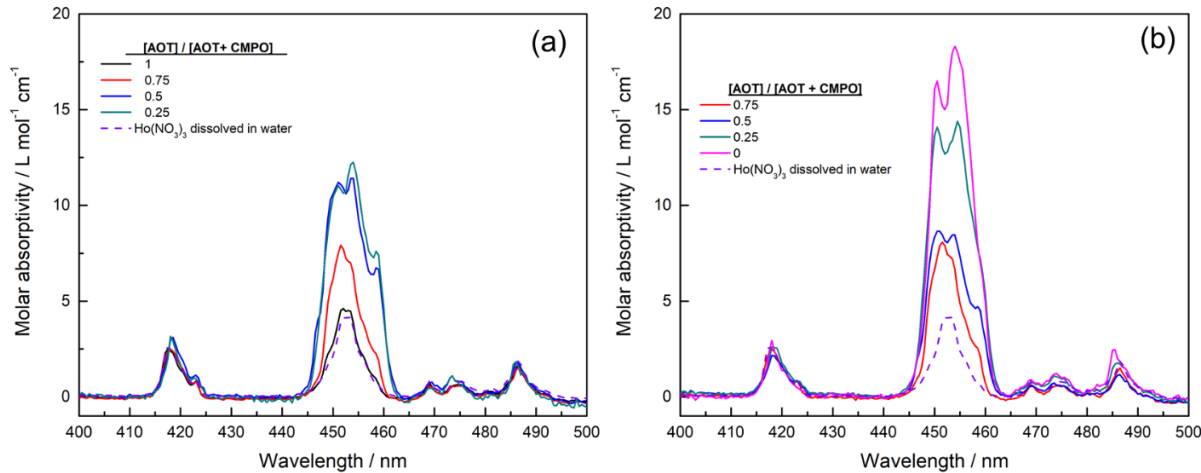
Figure 3.3 UV-vis absorption spectra of the organic phase after extraction varying extractants concentrations (legend shows the ratio of [AOT]/([AOT+CMPO])) with the aqueous phase including Ho^{3+} in (a) 0.001 M HNO_3 and (b) 0.5 M HNO_3.
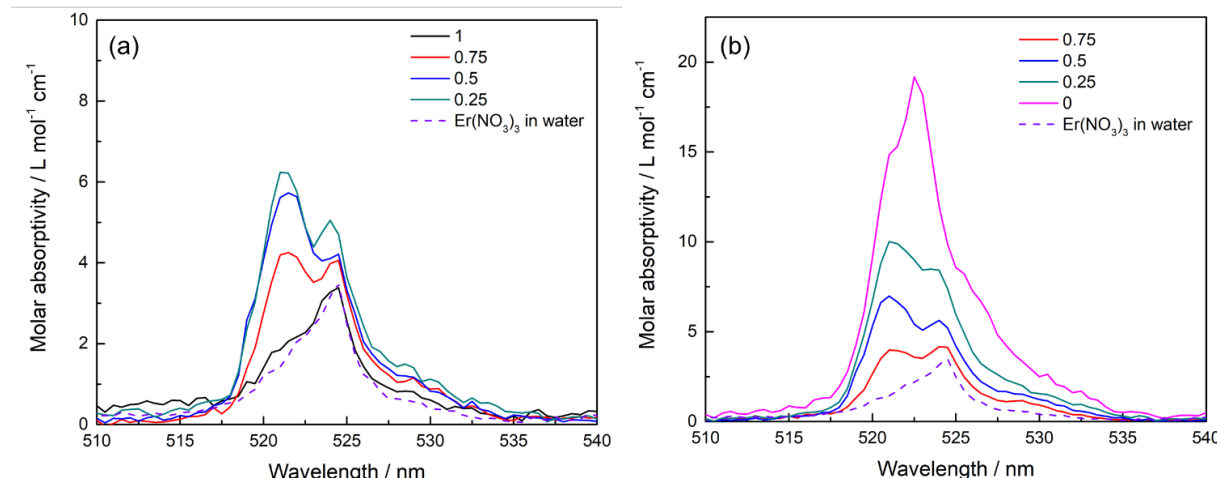
Figure 3.4 UV-vis absorption spectra of the organic phase after extraction using varying extractant concentration ratios with the aqueous phase including Er^{3+} in (a) 0.001 M HNO_3 and (b) 0.5 M HNO_3.

The extractability of metal ions increase in highly acidic solution and the extraction

is also possible from lower acidic medium if nitrate anion coexists in a sufficient

concentration[60-61]. Based on this extraction mechanism, CMPO cause asymmetrical

conditions around lanthanide ions resulting in the high absorbance of the hypersensitive

band. It is worth noting that the holmium absorption in the CMPO organic phase decreases when using 5 M HNO_3 in the aqueous phase. Although high nitric acid promotes Ho extraction CMPO may also extract nitric acid which cause the amount of CMPO available to complex metal ions to decrease. This is likely the reason for the low absorption of Ho in the organic phase when contacting with 5 M HNO_3, see figure 3.2b.

The UV-Vis spectrum of the organic phase including extracted Ho^{3+} or Er^{3+} with AOT-CMPO mixed system was measured for all different AOT ratios except for the case of CMPO itself (AOT ratio of 0) at low acid concentration (0.001 M) and AOT itself (AOT ratio of 1) at high acid concentration (0.5 M HNO_3) due to the low concentration of metal in the organic phase for those two conditions. Figure 3.3 shows the spectra from the organic phase, containing different AOT and CMPO concentration ratios, after contact with an aqueous phase containing 0.01 M holmium nitrate. Only the hypersensitive band is shown in Figure 3.3. The difference between Fig 3.3. (a) and (b) is the acid concentration in the aqueous phase. For low acid concentration, the spectrum of the holmium nitrate dissolved in the aqueous phase and the spectrum of holmium extracted with only AOT shows the same band shape structure. However, once the AOT ratio decrease, the intensity of the peak around 450 nm increase and split into three peaks. When the AOT ratio is less than 0.5, the band shape did not change and showed similar intensity. This suggest that AOT itself extract holmium from the aqueous phase as a hydrated form into the water core of the reverse micelle and not as a complex with AOT. As the AOT ratio decrease, CMPO substitutes the water and form complexes with holmium ion. For the organic phase with high AOT ratio (0.75) contacted with high acid concentration, the band shape is similar to the low acid concentration band shape. However, once AOT ratio decrease to 0.25, the band

shape turns into the double peak band similar to Ho extracted with CMPO only. Furthermore, the intensity of the peak in the organic phase containing high CMPO concentration is twice that of the peak for Ho extracted with AOT itself which can be explained by the symmetry of the lanthanide ion, as discussed above.

Similar to the holmium studies, erbium was also tested with different concentration ratio of AOT and CMPO contacted with aqueous solutions of different acid concentration. Erbium exhibits a hypersensitive absorption band between 520 to 525 nm owing to the $^4I_{15/2} \rightarrow {^2H_{11/2}}$ transition. Figure 3.4 shows the UV spectra of the organic phase following extraction with different AOT ratio at two different HNO_3 concentrations. When erbium was extracted with AOT by itself, the band shape is identical to the erbium nitrate aqueous solution (black and dashed purple lines in Fig. 3.4 (a) for AOT extraction and Erbium in aqueous phase, respectively). This indicate that AOT itself extract erbium in a symmetric hydrated form. This is directly comparable to the case of Ho extraction by AOT as discussed above.

However, when the AOT ratio is 0.75 or less, a second peak centered at 521 nm appeared, effectively forming a double peak. The intensity of the lower wavelength peak (at 521 nm) increase with decreasing AOT ratio. For extraction of erbium from high acidic aqueous solution using only CMPO, the band shape and intensity of erbium is significantly changed (Fig 3.4 (b) AOT ratio = 0) and show a peak centered at 523 nm with a small shoulder at 521 nm. This indicates that the complex formed between CMPO and erbium nitrate cause an asymmetric condition around Er^{3+}.

The significant band shape change observed in the UV-Vis data with different AOT ratio can be explained by changes in the surrounding environment of lanthanide such as

different coordinating molecules or change in coordination number. Increasing the polarity

of the ligand increases the intensity of the f $\rightarrow$ f transition band because the electron

donating ability of the ligand influence the f $\rightarrow$ f transition in the same direction which is

affected by the polarizing power of the surrounding anion in the second coordination

sphere of the lanthanide ion. Also, the band shape changes with different coordination

number because of the possible distortion caused by the nearest neighbor cation. Finally,

bound hydrated water ions may affect the spectral change[30, 32].

The $k^3\chi(k)$ EXAFS data and the corresponding Fourier transform (FT) data for the

extracted Ho with different AOT ratio from low and high acid concentration of the aqueous

phase are shown in Fig. 3.5. For the data for higher acid concentration, only AOT ratios of

0.75 and 0.5 are included in this study due to the low concentration of extracted holmium

in the solution. For AOT itself (AOT ratio = 1), the k-space and R-space data looks similar to

holmium nitrate dissolved in water. For CMPO itself (AOT ratio = 0), the data showed

different feature compared to the organic phase using AOT which showed a wider and

deeper oscillation peak around 2 Å^{-1} and a double peak signal at around 4 Å^{-1}. As the CMPO

concentration in the mixture increase, the features observed using CMPO by itself gradually

appeared. For higher AOT ratio, the FT data of the organic phase shows an intense peak at

1.9-2.0 Å (before phase shift correction) attributed to the nearest O neighbors. The peak

around 2.5 Å for AOT itself and 75% of AOT mixture is more likely a back-scattering

oscillation feature rather than second coordination feature due to multiple small peaks.

However, for lower AOT ratio, two peaks of physical significance appear. The additional

peak located at 3.3~3.45 Å (before phase shift) is attributed to the distant P atoms from the

second coordination shell.
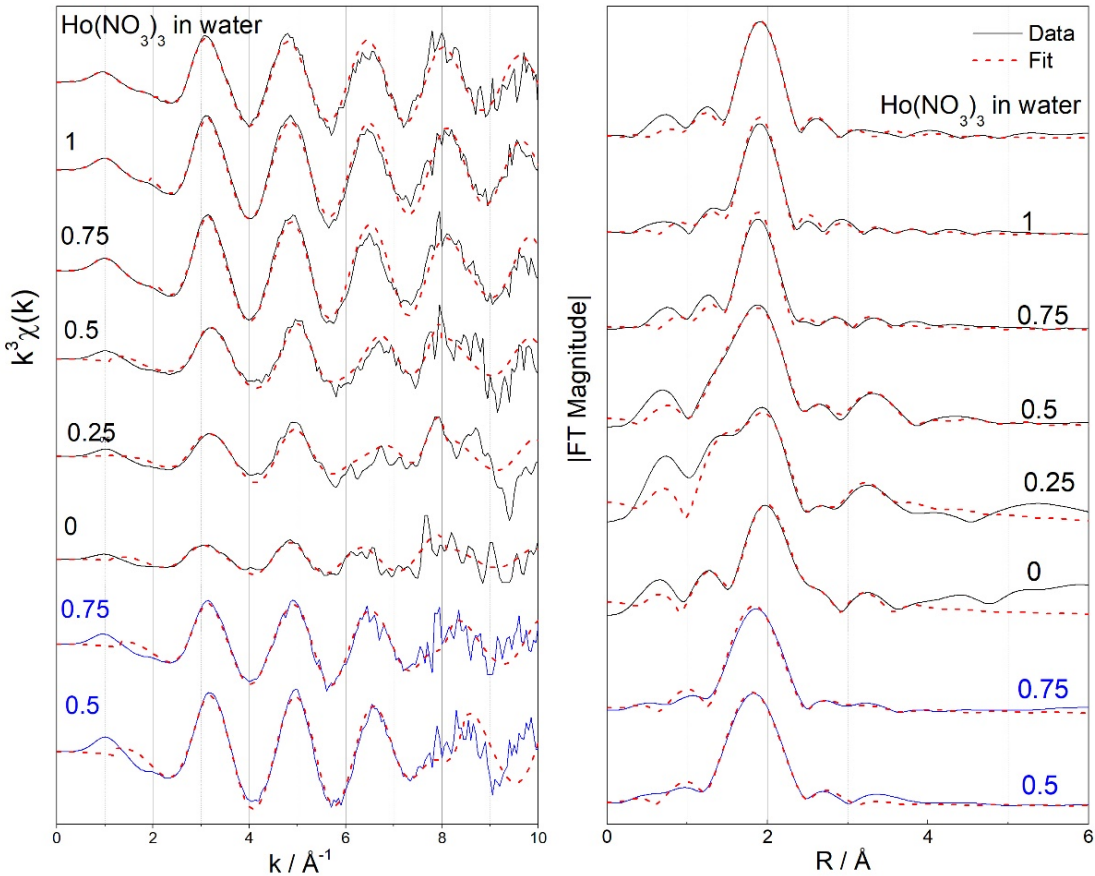
Figure 3.5 (Left) $k^3\chi(k)$ EXAFS data of organic phase extracting from aqueous phase containing 0.01 M Ho^{3+} with different composition of AOT and CMPO in 0.001 M HNO$_3$ (Black lines) and in 0.5 M HNO$_3$(Bottom two blue lines). (Right) Fourier transform data of the $k^3\chi(k)$ EXAFS (black) and the corresponding fits (red). The graph from the top box shows the organic phase after contact with holmium aqueous solution in 0.001 M HNO$_3$ and from the bottom box shows the contacted organic phase with holmium aqueous solution in 0.5 M HNO$_3$. The AOT ratio ([AOT]/[AOT+CMPO]) is given by each line.

For high acid aqueous concentration (Figure 3.5 bottom), the k-space data, plotted as k^3, show similar features at lower wavenumber for the two samples, but have different features at higher wavenumber. For 75% of AOT, the low k-space range showed similar properties with the organic phase extracted with AOT itself. However, for an AOT ratio of

0.5 a wider, double peak, feature was observed around 2 Å^{-1} which is similar to the organic phase at low acid with higher amount of CMPO.

Figure 3.6 shows the result of the k^3 weighted EXAFS data and corresponding Fourier transform data of the organic phase after contact with the aqueous phase containing 0.01 M Er in 0.001 M HNO$_3$. The organic phase with only CMPO was not analyzed due to its low extractability of erbium using low acid concentration. For the k-space data, two major changes are observed as the AOT ratio decrease. The oscillation around 4 Å^{-1} shifted slightly to higher wavenumber and the oscillation around 6 Å^{-1} gets wider as the AOT ratio decrease. The FT Er data shows an intense peak at 1.9-2.0 Å (before phase shift correction) attributed to the nearest O neighbors. However, for lower AOT ratio, an additional peak located at 3.3~3.45 Å (before phase shift) is observed, attributed to the distant P atoms from the second coordination shell. The associated linear least squared fitting of the EXAFS data of Ho and Er are shown in Table 3.1 and 3.2. The result of the fit indicate that Ho is close to 8-coordinate with O at 2.34 Å bond length of Ho-O for the organic phase with AOT by itself. This result is comparable to the holmium nitrate dissolved in the aqueous phase which showed similar coordination number and bond length. As the concentration of CMPO increase, the average distance of Ho-O decreased to 2.25 Å and the coordination number is also slightly decreased. This can be explained by the binding ligand changing from water to CMPO. When the holmium or erbium is bound with water the bond length between metal and oxygen are 2.34 Å. However, once CMPO binds with a lanthanide, the distance between oxygen from P=O of CMPO and lanthanide decreased. The erbium data also showed a similar trend as the holmium EXAFS data. In the literature, the coordination number and bond length of the erbium ion in the aqueous

phase are 7.4 and 2.33 Å, respectively[62]. Comparing this number to our result of the organic

phase contacted with the Er solution with low acid concentration showed similar bond

length and coordination number. As with holmium, when the CMPO concentration increase

the Er-O distance and coordination number decreased.

Table 3.1 Ho-O EXAFS fit results for organic solutions where Ho^{3+} was extracted from an aqueous phase with 0.001 M HNO_3. r is the interatomic distance, CN is the coordination number, σ^2 is the Debye-Waller Factor, ΔE is the energy threshold value, R-factor indicate the goodness of the fit.

		R / Å	err	CN	err	σ^2 / Å	err	ΔE / eV	err	R-factor
$Ho(NO_3)_3$ dissolved in Water	Ho-O	2.34	1.0E-03	8.3	0.017	0.00139	3.57E-05	0.369	0.005	0.0123
[AOT]/[AOT+CMPO] =1	Ho-O	2.34	4.30E-05	7.9	0.004	0.0005	1.67E-05	0.373	0.0005	0.0146
[AOT]/[AOT+CMPO] =0.75	Ho-O	2.35	2.80E-05	7.6	0.002	0.0007	8.09E-05	1.031	0.784	0.0130
	Ho-P	3.32	2.08E-02	0.2	0.301	0.0159	2.56E-02			
[AOT]/[AOT+CMPO] =0.5	Ho-O	2.25	1.00E-05	7.7	0.002	0.00097	1.11E-06	0.708	0.024	0.0158
	Ho-P	3.48	4.32E-02	0.5	0.328	0.0025	1.09E-03			
[AOT]/[AOT+CMPO] =0.25	Ho-O	2.25	3.54E-05	7.8	0.003	0.00529	1.39E-05	0.523	0.008	0.0135
	Ho-P	3.48	6.32E-02	3.0	0.043	0.000053	1.06E-04			
[AOT]/[AOT+CMPO] =0	Ho-O	2.25	2.03E-04	7.7	0.006	0.0053	1.24E-05	0.703	0.007	0.0129
	Ho-P	3.53	2.12E-03	3.0	0.173	0.0033	1.24E-04			

Table 3.2 Er-O EXAFS fit results organic solutions where Er^{3+} was extracted from an aqueous phase with 0.001 M HNO_3. r is the interatomic distance, CN is the coordination number, σ^2 is the Debye-Waller Factor, ΔE is the energy threshold value, R-factor indicate the goodness of the fit.

		R / Å	err	CN	err	σ^2 / Å	err	ΔE / eV	err	R-factor
[AOT]/[AOT+CMPO] =1	Er-O	2.34	4.30E-05	7.9	0.004	0.0005	1.67E-05	0.373	0.0005	0.01467
[AOT]/[AOT+CMPO] =0.75	Er-O	2.35	2.80E-05	7.6	0.002	0.0007	8.09E-05	1.303	0.914	0.0182
	Er-P	3.24	0.53E-02	0.1	0.404	0.0109	2.56E-02			
[AOT]/[AOT+CMPO] =0.5	Er-O	2.25	1.00E-05	7.7	0.002	0.0010	1.11E-06	0.413	0.012	0.0013
	Er-P	3.56	0.13E-02	1.0	0.132	0.0013	1.07E-03			
[AOT]/[AOT+CMPO] =0.25	Er-O	2.25	3.54E-05	7.8	0.003	0.00529	1.39E-05	0.372	0.027	0.0112
	Er-P	3.54	1.28E-02	3.0	0.782	0.00041	1.01E-04			

Table 3.3 Ho-O EXAFS fit results for organic solutions where Ho^{3+} was extracted from an aqueous phase with 0.5 M HNO_3. r is the interatomic distance, CN is the coordination number, σ^2 is the Debye-Waller Factor, ΔE is the energy threshold value, R-factor indicate the goodness of the fit.

		R / Å	err	CN	err	σ^2 / Å	err	ΔE / eV	err	R-factor
[AOT]/[AOT+CMPO]	Ho-O	2.26	3.15E-05	7.1	3.66E-05	0.006	2.53E-05	2.013	0.518	0.0116
= 0.75	Ho-P	3.50	1.01E-03	1	3.28E-01	0.01843	1.84E-02			
[AOT]/[AOT+CMPO]	Ho-O	2.25	1.23E-05	7.2	0.32E-04	0.0023	3.12E-05	1.206	0.051	0.0109
= 0.5	Ho-P	3.63	1.25E-02	3.0	5.0E-03	0.002825	1.72E-02			
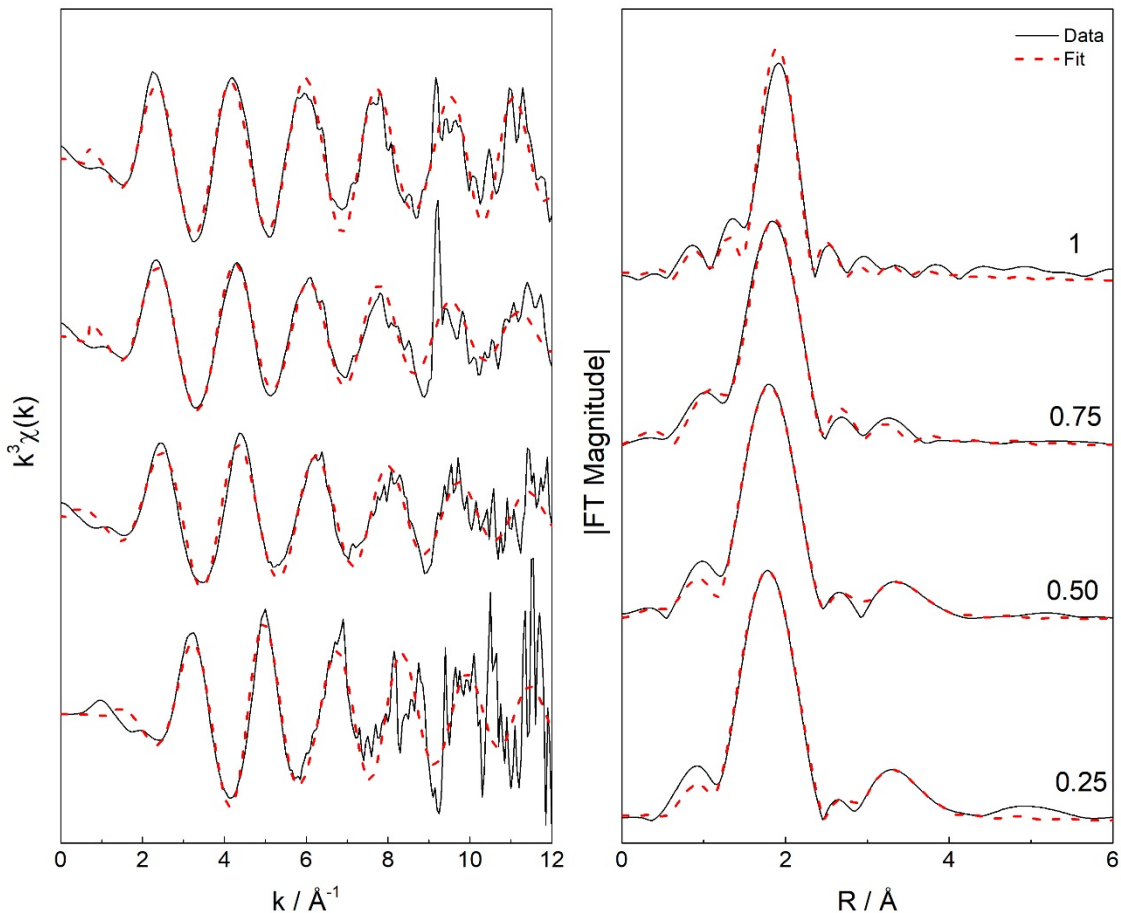
Figure 3.6 (Left) $k^3\chi(k)$ EXAFS data of organic phase extracting from aqueous phase containing 0.01 M Er^{3+} in 0.001 M HNO_3 with different composition of AOT and CMPO. (Right) Fourier transform data of the $k^3\chi(k)$ EXAFS (black) and the corresponding fits (red). The AOT ratio ([AOT]/[AOT+CMPO]) is given by each line.
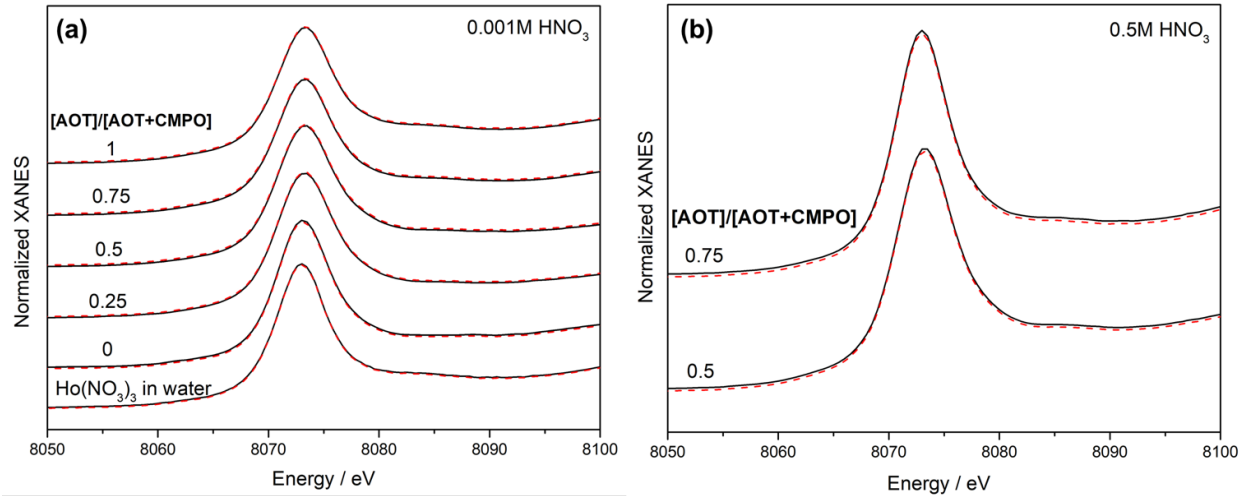
Figure 3.7 Normalized L-III edge XANES fitting for extracted Ho^{3+} in 0.001M HNO_3(left) and 0.5 M HNO_3 (right) Corresponding fits are shown as red dashed lines.

Table 3.3 shows the corresponding fitting result of the organic phase contacted with the aqueous phase including 0.5 M HNO_3. The EXAFS fitting result can be compared with the low acid aqueous concentration data from Table 3.1. When the AOT ratio is 0.5 for higher acid concentration, the distance of Ho-O is shorter, and the coordination number is smaller than for the lower acid concentration case. This can be explained by higher affinity with CMPO at high acid concentration in the aqueous phase. This indicate that CMPO contribute more to the extraction of lanthanides at higher aqueous acid concentration, as would be expected. The phosphorous atoms located in the second coordination sphere give a direct indication to the increased binding affinity of CMPO. It can be seen that when increasing the acid concentration in the aqueous phase the corresponding coordination numbers for the P atoms increase compared to the same AOT ratio at low nitric acid concentration. Furthermore, at an AOT ratio of 0.25 or below for the low acid case, and 0.5 for high acid, there appear to be three CMPO molecules surrounding the lanthanide ion.

This compares well with the stoichiometry reported previously for CMPO extraction of trivalent lanthanides and actinides from nitrate media[63-64].

Figure 3.7 shows the analysis of the Ho XANES, which provides further insight into the oxygen coordination environment surrounding the Ho center. The intense wide line of the normalized L-III edge XANES are characteristic of dipole-allowed electronic transitions from 2p to 5d for trivalent lanthanides30, and their general appearance suggest that the Ho^{3+} coordination environments are similar with different ratio of AOT in AOT-CMPO mixed system. Quantitative details were extracted from the XANES spectra by using the curve fitting in Table 3.4. The full widths at half maximum (FWHM) increased with decreasing AOT ratio which is attributed to the change in the coordination environment about the Ho center. This trend is caused by decreasing coordination number which correspond with the EXAFS fitting result.

Table 3.4 Parameters obtained from the XANES fitting for the organic phase including Ho^{3+}

Acid concentration	Sample	Center	err	FWHM	err	Height	err
0.001M HNO_3	[AOT]/[AOT+CMPO] = 1	8073.5	0.1	6.82	0.1	3.07	0.2
	[AOT]/[AOT+CMPO] = 0.75	8073.5	0.2	6.95	0.1	3.07	0.5
	[AOT]/[AOT+CMPO] = 0.5	8073.5	0.1	6.98	0.1	3.20	0.2
	[AOT]/[AOT+CMPO] = 0.25	8073.5	0.2	7.01	0.2	3.36	0.2
	[AOT]/[AOT+CMPO] = 0	8073.3	0.2	7.12	0.1	4.14	0.3
	$Ho(NO_3)_3$ dissolved in water	8073.5	0.1	6.09	0.2	3.68	0.2
0.5M HNO_3	[AOT]/[AOT+CMPO] = 0.75	8073.5	0.1	6.34	0.1	3.62	0.5
	[AOT]/[AOT+CMPO] = 0.5	8073.5	0.1	7.14	0.2	3.17	0.2
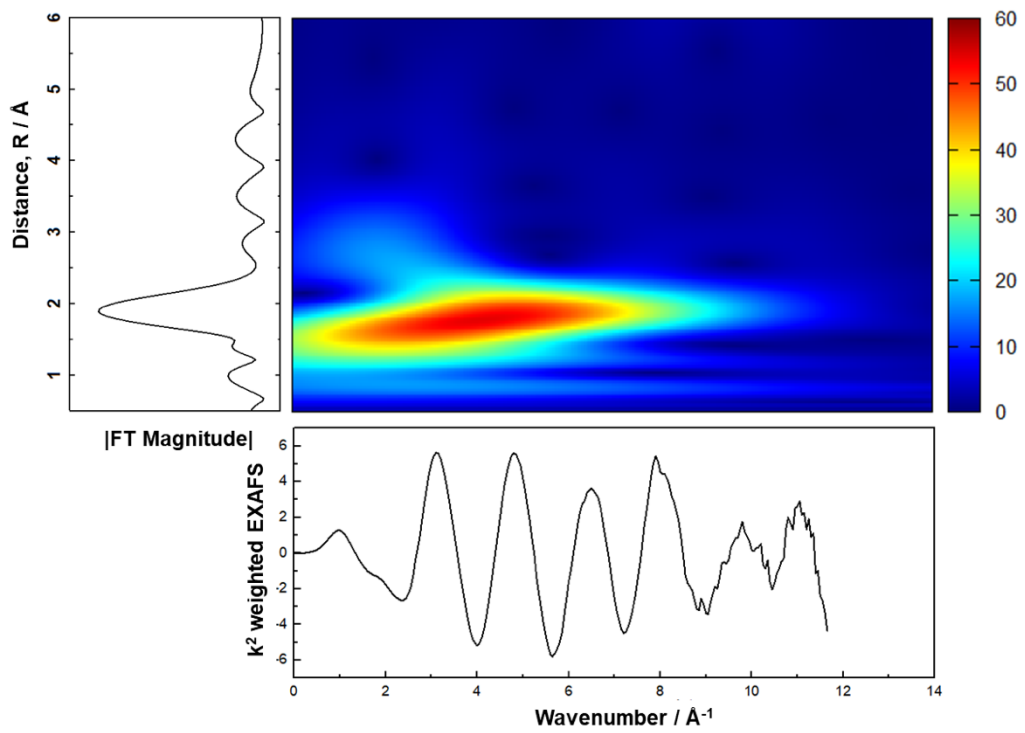
Figure 3.8 Overview of the wavelet transform modulus of holmium nitrate in the aqueous phase analyzed at Ho L-III edge; k-space spectrum (bottom panel), magnitude of its Fourier transform (left panel) and its Morlet wavelet transform (central panel)
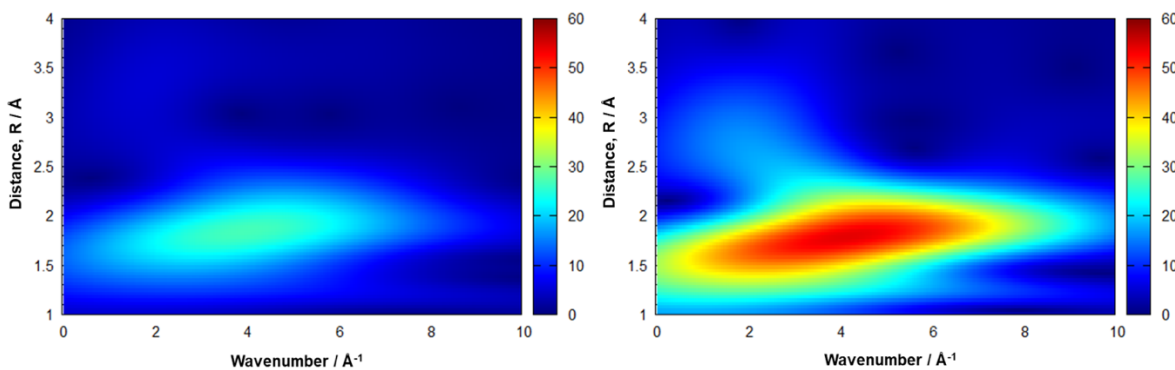
Figure 3.9 Wavelet transform modulus for (a) $Ho(NO_3)_3 \cdot 5H_2O$, solid (b) $Ho(NO_3)_3$ dissolved in water.

To further understand the EXAFS signal for the system, wavelet transform analysis was performed for each sample. Figure 3.8 shows the overview of the wavelet transform of

holmium nitrate in the aqueous phase. Traditional EXAFS analysis needs two separated k-space and R-space graphs to qualify or quantify the data, but by combining two separate data into one contour graph, the difference caused from multi-scattering can be easily visualized. Wavelet transform contour plots were generated by decomposing the k-space and R-space (uncorrected for phase sift) signals. As a result, the wavelet transform provides detailed information on the local structure with the visualized signal which are difficult to identify with two separate graphs. Also, for Fourier transform, it is hard to separate different back scattering atoms in higher coordination shells present at similar bonding distance from the central lanthanide atom. Wavelet transform facilitates the identification of the backscattering atom and allow to filter out the experimental noise and can show the disorder of the structure. The color intensity is proportional to the modulus that correspond to the EXAFS amplitude term[55-56, 65].

Figure 3.8 shows the spectrum of holmium nitrate dissolved in an aqueous phase. The major colored area shows the contribution from the Ho-O coordination shell. The location of the highest intensity for Ho-O in k-space were ~4.5 Å^{-1} and showed longer length contribution (between 2-3 Å in R-space). This higher length contribution is possibly coming from the Ho-O-N contribution of the nitrate since the Ho-N showed very weak intensity at 2.3 Å in R-space and strong oscillation occurred between 2 and 4 Å^{-1} in k-space. Because of the different backscattering atom from the higher coordination shell, the Ho-O scattering from each nitrate, P=O, and water showed different oscillation feature in k-space causing the different R space feature of Ho-O. This can be easily visualized through wavelet transform by analyzing the deformation of the Ho-O feature. The highest intensity of this Ho-O coordination shell caused from the hydrated water is understood by comparing the

WT result of $Ho(NO_3)_3 \cdot 5H_2O$ solid and $Ho(NO)_3$ aqueous solution (Figure 3.9). For solid holmium nitrate, uniform weak intensity was observed due to Ho-O from weakly combined water. Once dissolved in water, the strong Ho-O from the hydrated water appeared for the holmium nitrate aqueous solution.

Before examining the data from the extraction experiments, WT EXAFS modules for each possible Ho-O from hypothetical structures were simulated as references. The use of theoretical standards has become the preferred XAFS analysis and can accurately model multiple-scattering contribution as well as single scattering using reliable algorithms such as FEFF[58, 66]. If the Ho-O distance changed, the scattering path is shifted slightly but scattering oscillation will be the same in k-space. However, if the connected oxygen source from Ho are different (i.e. N from the nitrate or P from the CMPO P=O bond), the backscattering from the multiple scattering amplitude and phase changed with the higher coordination shell due to its element specific properties. Figure 3.10 is the simulated WT transform of Ho-O single scattering path with additional multiple-scattering path from different oxygen sources such as nitrate, water and phosphate. Ho-O from water (Fig. 3.10 (a)) shows a horizontally wide elliptic shape without any distortion over 1.2-2 Å radial distance and showed high intensity at the center of the shape. However, once the backscattering atom from higher coordination shell is changed into N, C or P the structure is not same anymore. When the backscattering atom is the nitrogen from the nitrate, the vague low intensity increased at lower wavenumber and higher radial distance (white arrow at Fig 3.10. (b)) and the center density decreased. For the case when P is the backscattering atom, two different scattering models (monodentate binding of one phosphate and bidentate binding with C=P and P=O from CMPO with holmium) were

visualized in Figure 3.10 (c) and (d). It is noteworthy that a wide low intensity circle area is observed between 4-6 Å^{-1} and 2-3 Å radial distance for monodentate structure while the bidentate oxygen bond from CMPO showed high intensity area at 6-9 Å^{-1} (2-3 Å radial distance).
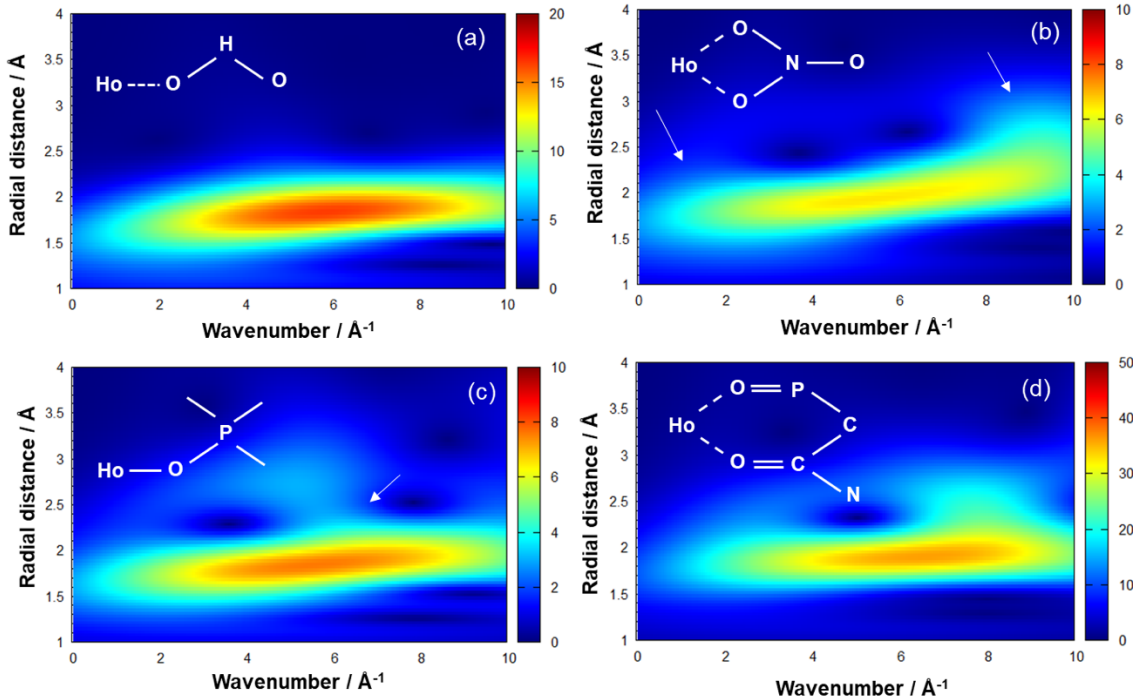
Figure 3.10 Simulated WT EXAFS model for Ho-O from different second backscattering atoms. (a) water, (b) nitrate, (c) monodentate binding of one phosphate and (d) a bidentate complexation of C=O and P=O from CMPO with Holmium. Each model includes Ho-O, Ho-P single scattering (for (c) and (d)) and double scattering of Ho-O-H (a) or Ho-O-N (b) or Ho-O-P (c) and Ho-O-P and Ho-O-C (d). Note that the contour density scale is different for each graph.
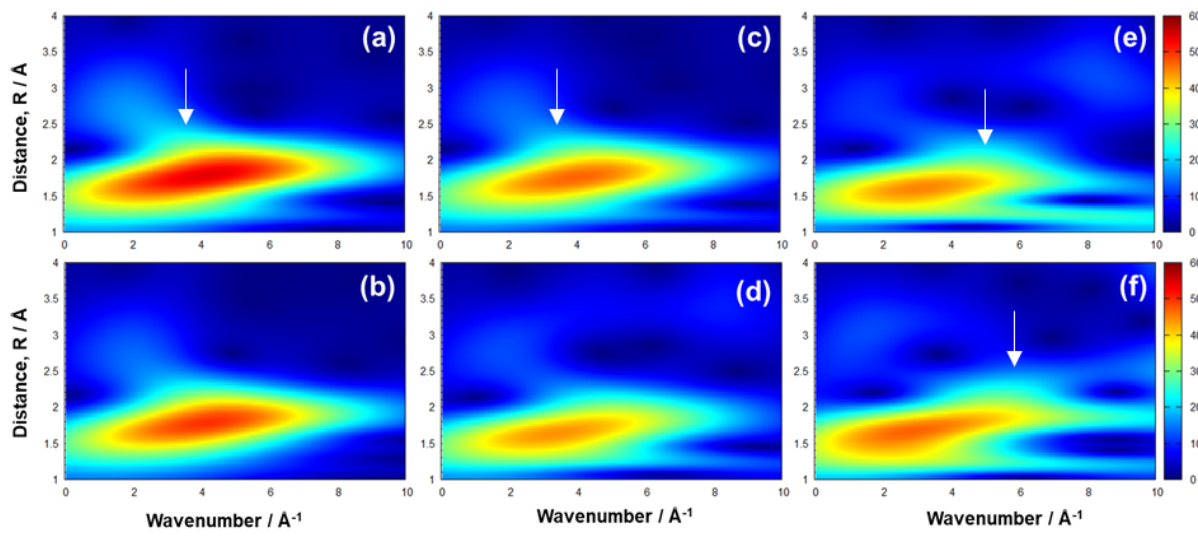
Figure 3.11 Wavelet transform modulus for (a) Ho(NO$_3$)$_3$ dissolved in water, (b) [AOT]/([AOT]+[CMPO]) = 1, (c) [AOT]/([AOT]+[CMPO]) = 0.75, (d) [AOT]/([AOT]+[CMPO]) = 0.5, (e) [AOT]/([AOT]+[CMPO]) = 0.25, and (f) [AOT]/([AOT]+[CMPO]) = 0 extracted with low acid concentration in the aqueous phase, plotted as a function of k (Å^{-1}) on the x-axis and R (Å) on the y-axis in the range of 1 to 4 Å.
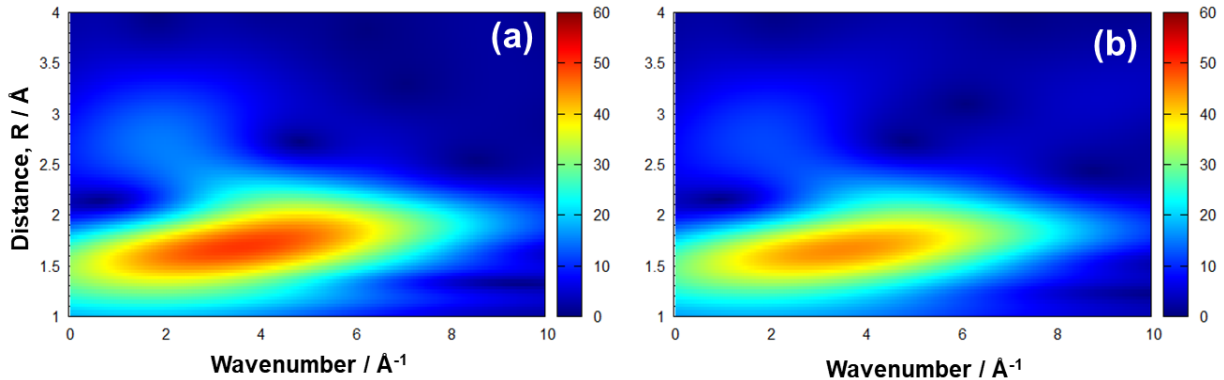
Figure 3.12 Wavelet transform modulus for (a) [AOT]/([AOT]+[CMPO]) = 0.75, (b) [AOT]/([AOT]+[CMPO]) = 0.5 contacted with high acid concentration in the aqueous phase, plotted as a function of k (Å-1) on the x-axis and R (Å) on the y-axis in the range of 1 to 4 Å.

Based on these reference spectra, the WT EXAFS data of the organic phase can be examined. Figure 3.11 show the organic phase contacted with the low acid aqueous phase. After holmium was extracted with the AOT itself, the shape and location are similar to the

aqueous holmium nitrate sample, but the intensity decreased due to the difference in solvent beyond the hydration shell. However, the intensity of the Ho-O from the water decreased as the AOT ratio decrease, owing to the loss of water in the reverse micelle, confirmed by KF titration. It is interesting to note that the intensity at the higher wavenumber (5-6 $Å^{-1}$) from second coordination shell increases at lower AOT ratio (Fig. 3.11 (e), (f) white arrow). This can be explained by formation of M-O-P bonds with CMPO. For AOT ratio of 0.5, the intensity of the second coordination shell (wavenumber = 2.7 $Å^{-1}$) show a slight shift to higher wavenumber although the bidentate mode does not appear dominant at the organic phase with 0.5 of AOT ratio. Figure 3.12 shows the wavelet transform EXAFS of the organic phase contacted with high acid concentration in the aqueous phase. The signal intensity from the coordination shell at $k \approx 3$ $Å^{-1}$ ($R \approx 2.3$ Å) is decreasing and shift to higher wavenumber compared with low acid concentration (Figure 3.11. (b), (c)). The shift to higher wavenumber is due to increasing binding ability of CMPO at higher acid concentration.

In the present work, the extractability and coordination chemistry of AOT and CMPO binary extraction system was studied. The system is known to display a cooperative effect at low concentration of each extractants, but the extractability did not increase remarkably by mixing two extractant when contacting with an aqueous phase with low acid content. The extractability increased by mixing the two extractants at higher acid concentration. However, the highest extractability of metal was observed using AOT by itself at low (0.001 M) acid concentration.

3.3 Conclusion

The coordination structure of lanthanide ions in this binary extraction system was studied using UV-Vis and XAFS analysis. AOT appear to extract lanthanides through reverse micelles and the extracted lanthanide exist as a hydrated ion. CMPO bind with lanthanides to form a complex with bidentate mode with C=O and P=O and decreased the amount of the hydrated water. This difference caused a significant change of the electron configuration observed in the hypersensitive f-f transition band of the lanthanide. However, when the same amount of AOT and CMPO were applied in the system, the spectroscopic properties showed the partially complexed properties with CMPO as a reverse micelle form resulting in stable phase and increased distribution ratio. This study suggests that CMPO prevents the formation of massive micelles in the aqueous phase by partially complexing with the trivalent metal ion in the aqueous-organic interphase and aiding in the formation of reverse micelle in the organic phase.

CHAPTER 4. A SAXS STUDIES OF AGGREGATION IN THE AOT-CMPO EXTRACTION SYSTEM

As was shown in Chapter2, AOT (Aerosol OT) shows reasonable extractability of holmium but is unstable under extraction condition due to the formation of third phase or emulsion phase in either aqueous or organic phase. In further studies incorporating CMPO (carbamoylmethylene phosphine oxide), we showed that the combination of AOT and CMPO display synergistic effect not only in respect of the extractability of metal ions but also on the stability of both phases by reducing the propensity to form third phase or an emulsion phase. From traditional molecular-level understanding through a study of the coordination chemistry of the AOT-CMPO system, we observe that that complexation from the CMPO is aiding the control of water extraction through reverse micelles by AOT, resulting in a cooperative effect of certain mixtures of AOT-CMPO. However, the structure of these mixed aggregates and how it may affect synergy is not possible to observe from our molecular-level study, i.e. from X-ray and UV-visible absorption spectroscopy.

In this chapter, we investigate the properties of the aggregates formed with different concentration ratio of AOT and CMPO and the effect of acid concentration in the aqueous phase, focusing our investigation on collecting small angle X-ray scattering (SAXS) data. Various analysis methods of the SAXS data were applied including generalized indirect Fourier transformation (GIFT) method[40] to elucidate the effect of shape and size of the reverse micelle in the mixed-extractant domain.

4.1 Experimental method

Aqueous solutions of 0.01 M of holmium were prepared by first dissolving holmium oxide (99.999%) provided by Michigan Metals & Manufacturing, in nitric acid to prepare a stock holmium nitrate solution that could then be diluted to appropriate concentration. Concentrated nitric acid (15.8 M) was supplied by Marcon Fine Chemicals. Water used to dilute concentrated solutions was obtained from an in-house source of ultrapure (18.2 MΩ·cm) water. Sodium nitrate was obtained from Fischer Scientific and was filtered and recrystallized before use. Aqueous solution for the extraction studies were prepared by diluting the holmium stock solution to appropriate concentration in nitric acid. These solutions were subsequently standardized for Ho^{3+} concentrations, acidity (H^+ concentration) and excess nitrate concentration by a combination of neutron activation analysis, potentiometric titration, and ion chromatography. Sodium docusate (AOT) anhydrous was obtained from Fisher Scientific to >99% purity. CMPO was obtained at 96 % purity from Marshallton. Organic solutions containing different concentration of AOT and CMPO were prepared by dissolving a suitable amount of each reagent in heptane (HPLC grade, >99.0 %) obtained from OmniSolv. The organic chemicals were all used without any further purification.

Solvent extraction experiments using AOT and CMPO in heptane were performed by contacting equal volumes of the organic and aqueous phase for 10 min using a vortex mixer followed by centrifugation at 3000 rpm for 3 min. The distribution ratios of Ho were determined by neutron activation analysis using UC Irvine TRIGA® reactor. The holmium was activated to produce 166Ho and the activated samples were analyzed using a High Purity Germanium (HPGe) detector (30% relative efficiency, Canberra).

To investigate the aggregation feature with different concentrations of AOT and CMPO, we applied three different concentration combinations of AOT and CMPO; (1) varying [AOT] with constant [CMPO], (2) varying [CMPO] with constant [AOT] and (3) constant total concentration of AOT and CMPO at 0.1 M and varying ratio of AOT to CMPO. After contact with an aqueous phase, water concentration in the organic phase was determined with Karl Fisher titrations using a Metrohm KF Titrando with each sample measured in duplicate. The Karl-Fisher measurements were checked for accuracy using standardized solutions of 1 mg water per 1 g solution, HYDRANAL® Water Standard 1.0 obtained from Fisher Scientific. Also, different nitric acid concentration was used in the aqueous phase to see how the nitric acid concentration effects the synergic effect of combining CMPO and AOT.

SAXS was performed at the Advanced Photon Source (Argonne National Laboratory) at beamline 12-ID-C where the 18 keV incident X-ray beam was monochromatized providing good X-ray transmittance for all solution systems. Samples were contained in 2 mm diameter quartz capillary tubes (Charles Supper Co., 20-QZ). The sample-to-detector distance was adjusted to provide a detecting range for momentum transfer of $0.01 \leq q \leq 0.5$ Å^{-1}, where q was calibrated using a silver behenate standard. Background subtraction of the heptane solvent and the capillary tube was performed with a single capillary tube for each sample to obtain data without capillary-to-capillary variation. The final scattering curve was obtained from the subtraction of the capillary and solvent. The SAXS data, I(q), a function of the momentum transfer $q = (4\pi\sin\theta/\lambda)$, where 2θ is the scattering angle and λ is the wavelength of the incident X-ray beam, were plotted against q / Å^{-1}.

4.2 Result and discussion

The first extraction set was with fixed AOT concentration at 0.05 M and varied the CMPO concentration from 0.01 to 0.07 M. Figure 4.1 (a), (b) shows the distribution ratio and water contents of organic phase after extraction. With 0.01 M holmium nitrate in the aqueous phase with low acid concentration (0.001 M), it showed non-linear distribution of holmium with the highest distribution ratio observed at 0.03 M AOT concentration. When 0.5 M nitric acid was used, the distribution ratio also shows non-linear trend with the highest distribution ratio observed at 0.01M AOT concentration. At high acid aqueous concentration (3 M), holmium did not extract well although the distribution ratio slightly increases as the CMPO concentration increased to 0.05M. At low CMPO concentration (0.01 M), the distribution ratio improved for 0.5 M HNO_3 compared to low acid aqueous phase (0.001M HNO_3). It showed synergistic effect at low CMPO concentration(0.01M~0.03M) with 0.05M AOT compared with AOT itself. At the highest acid concentration, AOT extracted poorly compared to low acid due to deformation of the structure however a slight increase in the distribution ratio was observed at high CMPO concentration which is expected due to its improved extractability of lanthanides by CMPO at high acid concentration in the aqueous phase. Water contents showed a similar trend as the metal ion distribution ratio except for the case of extraction using high CMPO concentration and high nitric acid concentration. At higher acid concentration (3 M), the water content was similar around 600~700 ppm, in all cases. However, the highest concentration of CMPO (0.07M) with AOT (0.05M) resulted in an aggregated third phase at high acid concentration (Fig. 4.2) with a total mass balance of 83.6 ± 1.7% for holmium for the organic phase and the aqueous phase. This could be explained by CMPO promoting a formation of polymeric

species as metal-extractant aggregates in the presence of high metal and acid concentration by bridging functional groups of the extractant molecules.

The second extraction set was with different AOT concentrations while keeping the CMPO concentration constant at 0.05 M. Figure 4.1 (c) and (d) shows distribution ratios and water content of the organic phase after extraction using different CMPO concentration. In the extraction from 0.001 M HNO_3 and 0.5 M nitric acid in the aqueous phase, distribution ratios increased with AOT concentration. We observed lower distribution ratios for 0.5 M HNO_3 compared to the lower acid case (0.001M HNO_3). Likewise, the water contents showed similar trends as the metal distribution ratio which may be explained by the extractability of holmium increasing with the formation of reverse micelles.
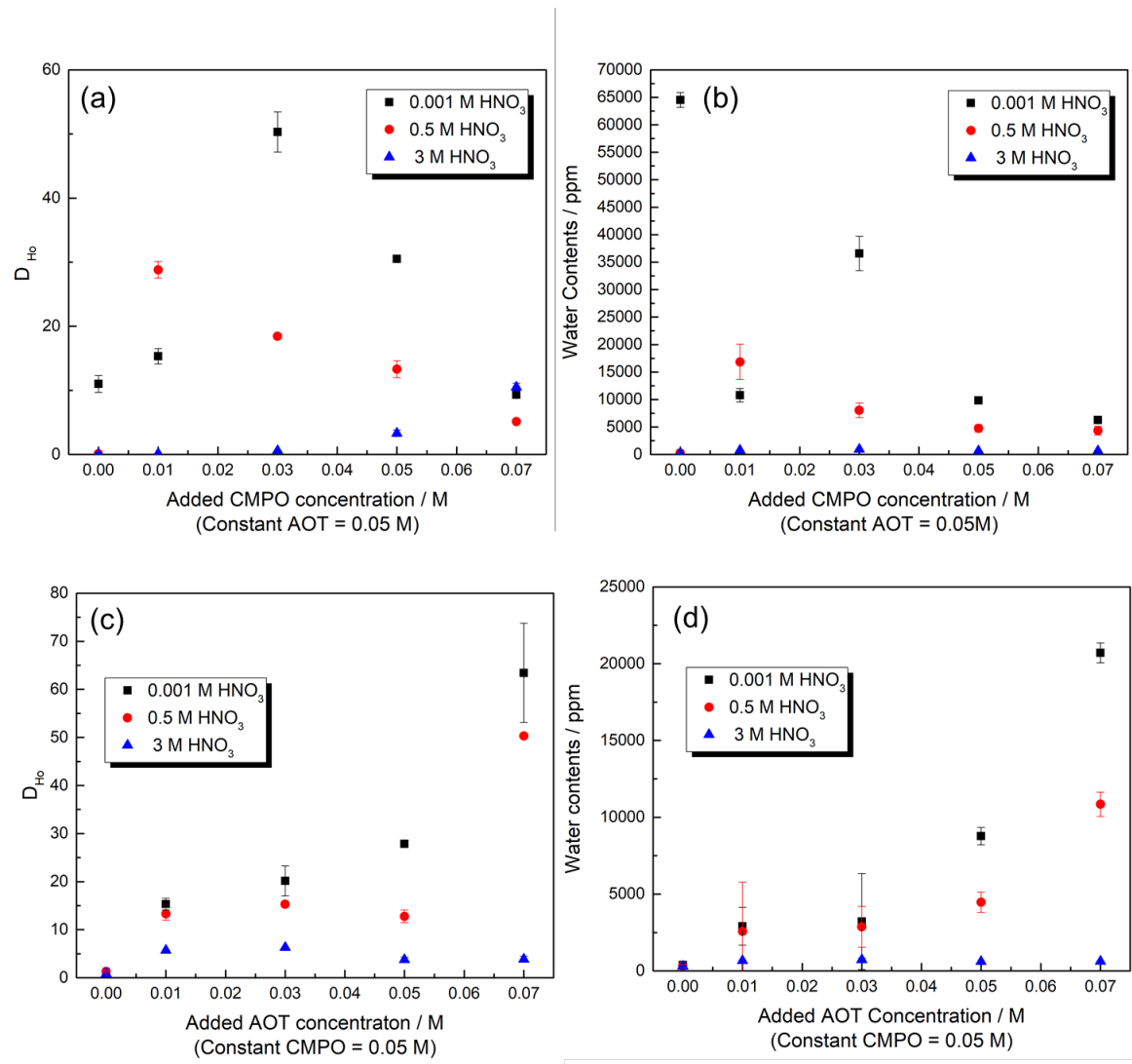
Figure 4.1 Distribution ratio of Ho (III) after extraction with 1×10^{-2} M Ho(NO$_3$)$_3$ dissolved in different concentration of nitric acid (black square = 0.001 M, red circle = 0.5 M, and blue triangle = 3 M) at (a) different CMPO concentration but constant (0.05 M) AOT concentration, (c) different AOT concentration but constant (0.05 M) CMPO concentration in heptane. Water content of the organic phase after extraction with (b) different CMPO concentration (constant AOT concentration) (d) different AOT concentration (constant CMPO concentration).
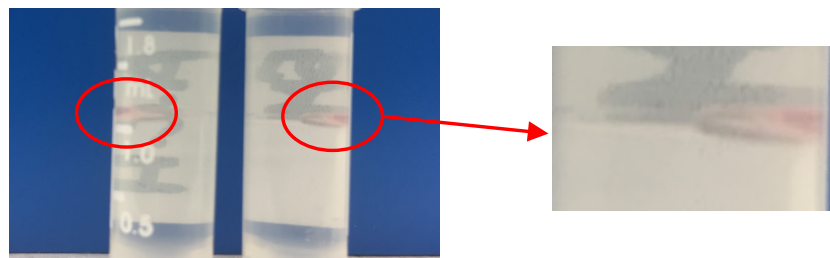
Figure 4.2 Precipitation observed in the phase boundary after extraction with CMPO (0.07M) and AOT (0.05 M) in high acid concentration (3 M HNO₃).
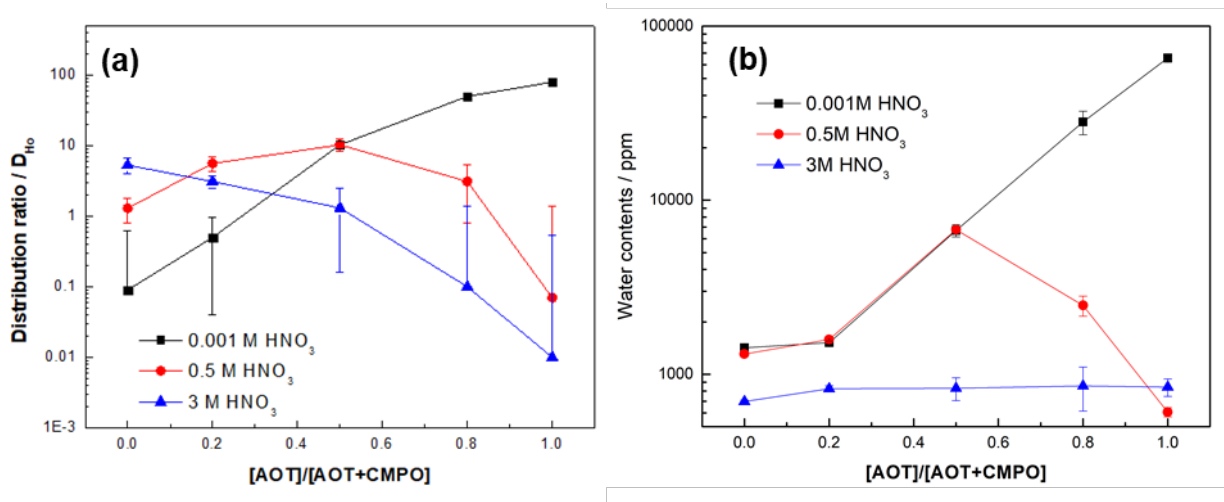
Figure 4.3 Distribution ratio (D_{Ho}) with different AOT and CMPO concentration ratio contacted with the aqueous phase including different acid concentration (0.001, 0.5 and 3M). Corresponding water contents of the organic phase showed at (b). Total concentration of the AOT and CMPO fixed to 0.1 M and changed the AOT and CMPO concentration ratio.

Finally, we tested different molar ratios of AOT and CMPO([AOT]/[AOT+CMPO] = 1, 0.8, 0.5, 0.2, 0) keeping total extractant concentration at 0.1M. As before, the organic phases were contacted with aqueous phases containing different acid concentration. For low acid concentration (0.001 M), the holmium distribution and water content increased with increasing AOT ratio, but at the AOT ratio of 1.0 showed massive emulsion formation in the aqueous phase while the organic phase remained clear. However, this emulsion in the aqueous phase disappeared as the AOT ratio decreased. For 0.5 M HNO₃, a non-linear trend

was observed for the holmium distribution ratio and water uptake. At the highest acid concentration, there was some extractability of holmium at low AOT ratio, while holmium did not extract at higher AOT concentrations. As mentioned above, this can be explained by the deformation of AOT at higher acid concentration while the extractability of holmium by CMPO is promoted by an increase in acid concentration[67-68].

SAXS measurements were collected from the organic phase before contact and after contact with the holmium aqueous phase for the low acid and high acid concentration experiments. The extraction result showed that the water contents depend on the AOT concentration due to microemulsion or reverse micelle formation. The principal contrast of the SAXS measurements is from the hydrocarbon oil against the electron-rich head group, extracted Ho^{3+} and extracted water in the reverse micelle. When compact reverse micelles exist, the scattering arises from the polar core but once larger water-in-oil aggregates form in the system, the scattering will arise from a shell of headgroups and counter ions, effectively located on the polar side of the interface[36, 47].
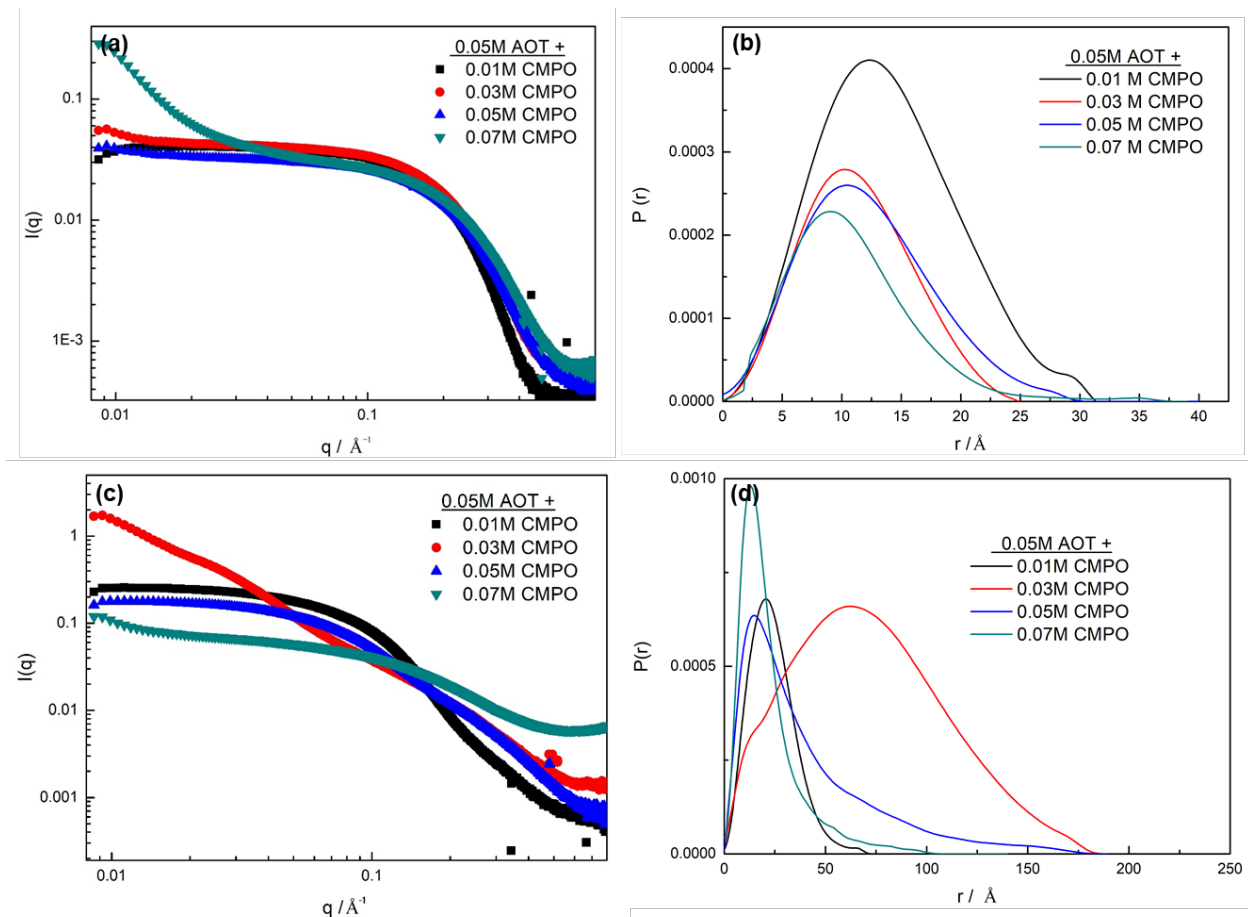
Figure 4.4 Log-log plot of the SAXS data for the 4 different CMPO concentration with constant AOT concentration before (a), and after (c) contact with an aqueous phase of 0.001 M HNO₃. Analyzed P(r) functions for each data set before (b) and after (d) extraction. The data for the solutions with different CMPO concentration are shown with the same color in I(q) and P(r) graph. Note the different scale between the figures.

Table 4.1 Maximum linear extent (MLE) and the inflection point obtained from the 1st derivative of the PDDFs (Figure 4) for the organic solution before and after contact with the aqueous phase containing 0.01M holmium nitrate in 0.001M HNO₃.

Added CMPO concentration / M	MLE / Å		Inflection point / Å	
	Before contact	After contact	Before contact	After contact
0.01	33	74	18.0	32.3
0.03	28	190	15.3	103
0.05	39	190	16.2	25.0
0.07	42	140	12.7	23

Figure 4.4 presents SAXS measurements on CMPO concentration effects with fixed AOT concentration (0.05 M) and pair distribution function of corresponding SAXS results. Fig. 4.4 (a) and (b) is the SAXS result of the organic phase before contact with the aqueous phase and (c) and (d) shows the result of the organic phase after contact with the aqueous phase containing holmium nitrate in 0.001 M HNO_3. Also, the maximum dimension of the aggregates or the length of the structure, which corresponds to the point at which the P(r) functions decay to zero showed as maximum linear extent (MLE)[47] and the inflection point of P(r) function obtained from the highest y-value of the first derivative serving as a semiquantitative measure of the internal structure such as cross-section of the reverse micelle[36, 47] were shown in table 4.1.

Before contact with the aqueous phase, an increasing trend of the I(q) in the low-q region with increasing CMPO concentration is observed, which is proportional to the higher-r side of the P(r) curves. As can be seen from the PDDF data, the r_{max} position, i.e. the position where the intensity is the highest, decrease with increasing CMPO concentration. However, the shape of the reverse micelle appears to be globular for all the samples with the exception of highest CMPO concentration where there is significant tailing after the first peak, suggesting elongated aggregates. Overall, this indicates that the reverse micelles may be shrinking with the addition of CMPO before contact with the aqueous phase. After contact with the aqueous phase, the extracted water and holmium cause drastic changes in the structure of the reverse micelle both in terms of their maximum size and the internal structure, i.e. shape of the micelles. The intensity close to I(0) increased compared to the organic phase before contact with the aqueous phase, with the exception of the highest CMPO concentration. It is noteworthy that the SAXS waves tend towards a straight line of

gradient -2 on the log-log plots for the 0.03 M CMPO with 0.05 M AOT, showing a power-law behavior of q^{-2}. Power law feature in the I(q) data can give qualitative insight into the structure of the aggregate in the organic phase; q^0 indicates globular reverse micelles, whereas q^{-2} indicates 2-dimentional superstructure[47, 69]. For the 0.07 M CMPO, the high range of q shows similar straight feature as for 0.03 M CMPO, while the low range of q shows q^0 feature with a similar inflection points as the organic phase of low CMPO (0.01 M). For the sample with the highest CMPO concentration, the intensity at low q range is the lowest although there is still some slight upward trend suggesting aggregation. The intensity at high q range is higher than the initial organic phase before contact with the aqueous phase. The P(r) function of the low CMPO concentration (0.01 M CMPO + 0.05 M AOT) showed a single bell-shaped curve with an extended tail to the high r-regime which indicates globular particles coexisting with rod shape aggregates no longer than 74 Å. For 0.03 M CMPO, the first peak more closed to shoulder of major peak showed at approximately 12 Å which is similar to the peak location for other CMPO samples. After this shoulder, a large, broad peak is observed in the higher-r region. This can be explained by strong attractive interaction between two different extractant[36, 47, 69]. This condition also resulted in the highest distribution ratio and water uptake. However, this effect decreased for the case when equal concentration of AOT and CMPO were applied in the system. For the 0.05 M CMPO, the pronounced peak in the low-r regime showed an exponentially decaying distribution into higher-r region which correspond to cylindrical shape. From the inflection point, the cross-section diameter was 25 Å with 190 Å of maximum dimension which suggest that the cross-section decreased as the CMPO concentration increased and longer aggregates are formed. For 0.07 M CMPO, the exponential distance distribution at

higher-r regime disappeared and displayed a more globular shape with slightly elongated tail, and the cross-section and maximum dimension (MLE) decreased to 23 Å and 140 Å, respectively. From these structural result and extraction result, the high extractability of the system containing 0.03 M CMPO with 0.05 M AOT may be caused by structural changes and attraction between the two different extractants.
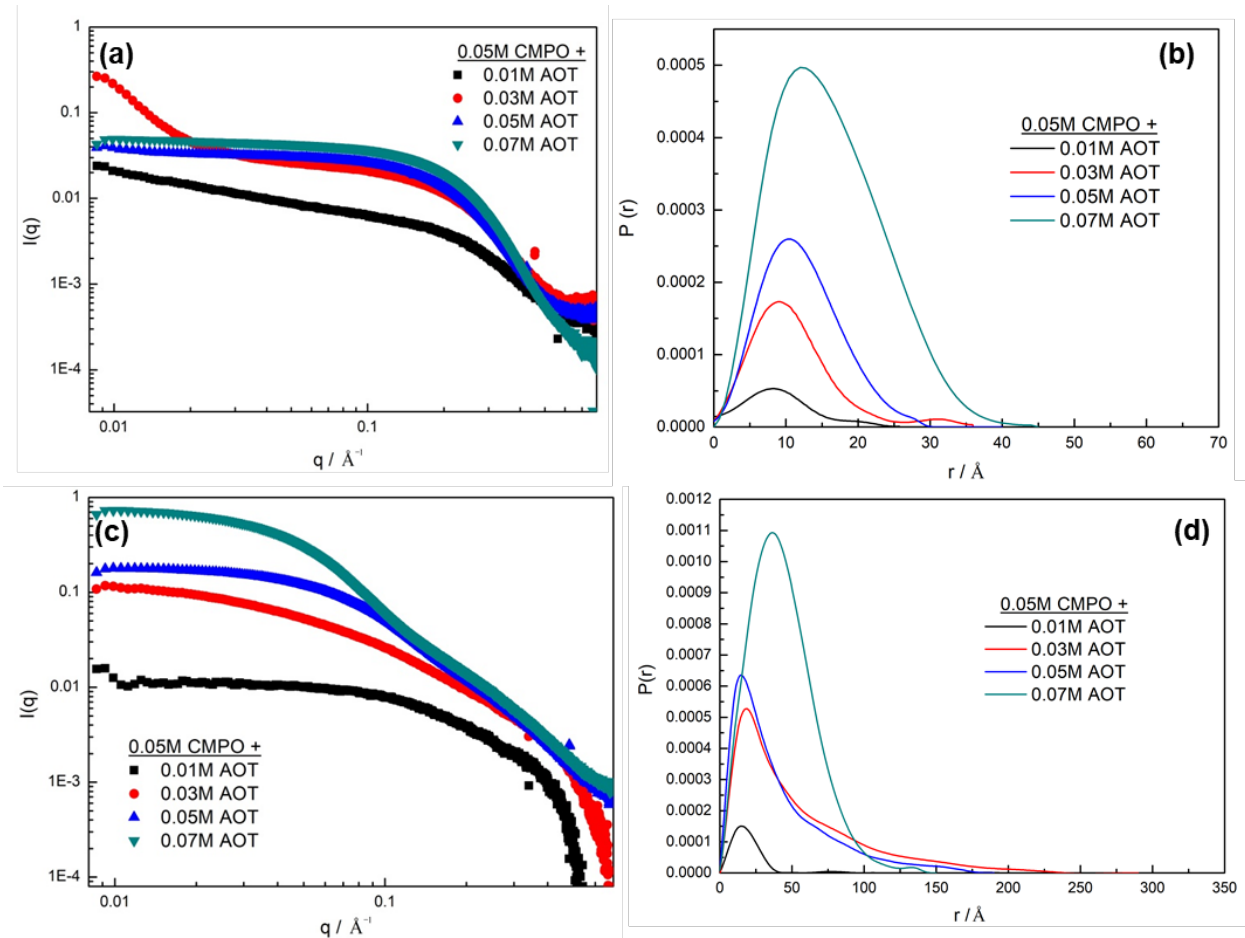
Figure 4.5 Log-log plot of the SAXS data for the 4 different AOT concentration with constant CMPO concentration before (a), and after (c) contact with 0.001 M HNO₃ aqueous phase. Analyzed P(r) functions for each before (b) and after(d) extraction. The data for the solutions with different CMPO concentration are shown with the same color in I(q) and P(r) graph.

Figure 4.5 shows results from the SAXS measurements with varying AOT

concentration and constant concentration of CMPO, effectively investigating the effect of

increasing AOT. The MLE and the inflection point of the P(r) graph are shown in table 4.2.

Before contact with the aqueous phase, a straight decreasing slope is shown for I(q) vs q

for the lowest AOT concentration (0.01 M AOT). The intensity increases for samples with

higher AOT concentration with a flat line observed at lower q region with the exception for

0.03 M AOT where an aggregation feature is observed. The P(r) plot showed a bell-shaped

curve with some additional peak features at higher r range which suggests a globular state

coexisting with short rods. Furthermore, there is an increasing trend for the peak intensity

with increasing AOT concentration with a peak center shift to higher r. This suggest that

AOT cause a size increase of the aggregates in the dry mixed-extractant systems. After

contact with the aqueous phase the shape of the I(q) graph changed drastically compared

with the organic phase before contact. For low AOT concentration (0.01 M), it did not show

and logarithmic dependence of I(q) vs. q and the inflection point showed at higher q range

suggest a small near-spherical reversed micellar aggregate. For 0.03 M AOT, the intensity

I(q) scales in the range 0.01 - 0.09 Å^{-1} as approximately q^{-1} which suggest long thin

cylindrical aggregates. As the AOT concentration increase to equal or higher than the

constant CMPO concentration, the logarithmic dependence of the lower q range

disappeared and there is no longer an exponent of -1 at low q. This structural information

is also shown in the P(r) function plot. At low AOT concentration (0.01 M), the P(r) function

is bell shaped which suggest spherical aggregates with slightly extended tail which caused

from the coexisting rod-shaped micelles, but for the 0.03 M AOT it suggests an elongated

cylinder feature which is seen by the pronounced peak in the low-r regime and an

exponentially decaying length distribution at higher-r regime. Also, the cross-section

dimension obtained by the second inflection point of the P(r) graph increase slightly as the

AOT concentration increased. However, the tailing feature at the higher r regime

disappeared once the AOT concentration increased to 0.07 M and showed a bell-shaped

feature with an extended tail suggesting that the aggregates take on a more spherical shape

with some mixed-rod-feature as the AOT concentration increases.

Table 4.2 Maximum linear extent (MLE), and inflection point obtained from the PDDFs
(Figure 5) for the organic solution before and after contact with the aqueous phase
containing 0.01M holmium nitrate in 0.001M HNO_3

Added CMPO concentration / M	MLE / Å		Inflection point / Å	
	Before contact	After contact	Before contact	After contact
0.01	25.7	240	10.29	26.43
0.03	38	290	13.90	27.35
0.05	40	190	15.97	25.27
0.07	45	150	24.77	13.18
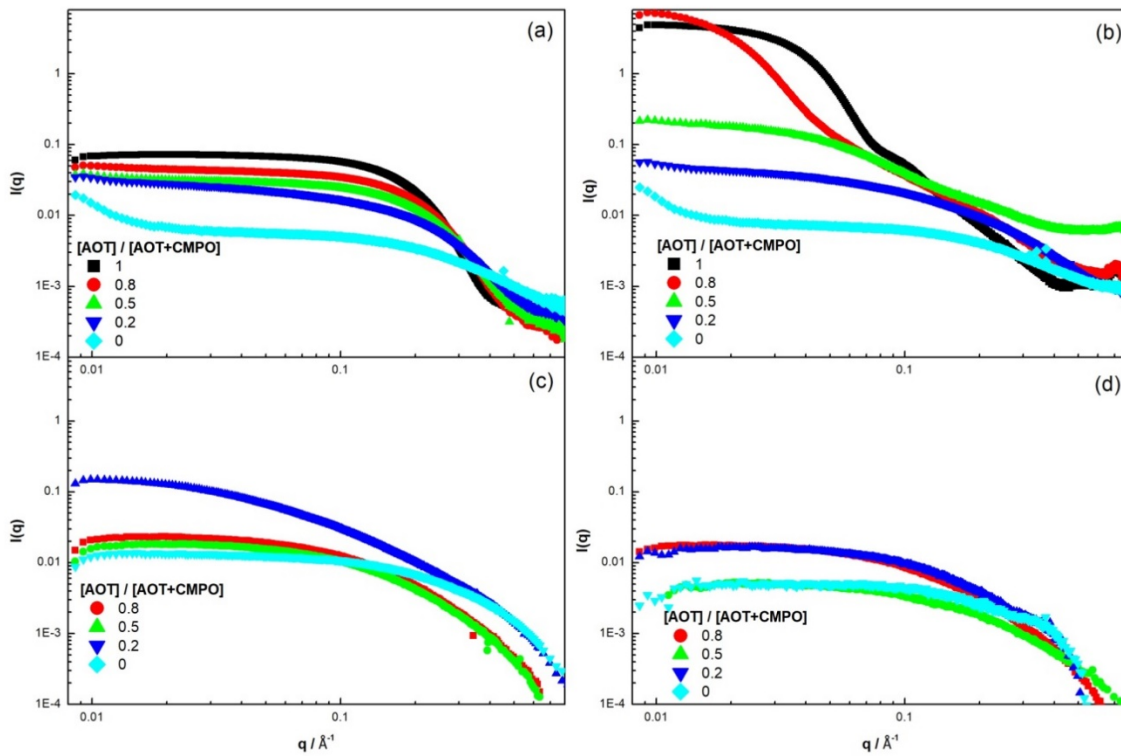
Figure 4.6 Log-log plot of the SAXS data for different concentration ratio (a) before contact with aqueous phase, (b) after contact with the aqueous phase containing 0.01 M Ho^{3+} in 0.001 M HNO_3 acid concentration, (c) after contact with the aqueous phase containing 0.01 M Ho^{3+} in 0.5 M HNO_3 and (d) after contact with the aqueous phase containing 0.01 M Ho^{3+} in 3 M HNO_3 aqueous phase. The mixture of 1 mol ratio of AOT for 0.5 M and 3 M is not included due to radiation damage during the measurement causing the low q region to increase in intensity between scans.

Figure 4.6 shows the I(q) profile of the organic phase that contained different molar ratio of AOT and CMPO (constant total concentration of extractants at 0.1 M) before and after contact with the aqueous phase containing Ho^{3+} with different acid concentration. Before contact with the aqueous phase, the I(q) slope changed slightly with the concentration ratio. The total intensity of the I(q) decrease and the inflection points are slightly shifted to higher q with decreasing AOT ratio. Also, the slope from the curve using

AOT itself is close to q^{-0} but with increasing CMPO concentration the slope power increases but does not quite reach q^{-1}. For CMPO itself, the slope is close to q^{-1} and the data suggest some aggregates feature close to I(0). These organic phase features before contact with the aqueous phase changed drastically after it was contacted with the aqueous phase containing Ho^{3+} especially in case of 0.001 M HNO_3. For an AOT ratio of 0.2 and 0, the scattering pattern did not change much compared to the dry organic phase, due to low extractability of CMPO at low acid concentration. However, the slope of the scattering pattern for an AOT ratio of 0.5 increases to q^{-1} which correspond to the elongated cylindric features. As ratio increased up to 0.7 and 1, the data suggest larger aggregate features with different scattering pattern.

After contact with the higher acid concentration, 0.5 M and 3 M, more or less similar scattering patterns were observed across all different AOT ratios. However, the inflection point shifted to higher r region for the AOT ratio of 0.2 and 0. Finally, for the AOT ratio of 0.2 contacted with 0.5 M HNO_3, the intensity in the low-r regime showed the highest value with a slope of the scattering pattern close to q^{-1}.

As before, these structural features from the I(q) was further investigated through the GIFT generated-P(r) functions. Before contact with the aqueous phase, the P(r) function of the different AOT ratios are bell shaped and the peak center shifted to lower-r except for the case of CMPO by itself (AOT ratio = 0). The P(r) function of the CMPO itself showed a bell shape slight shift to the right and with a long tail explained by MLE, which suggests the globular aggregates coexisting with rod shaped aggregates. After contact with the aqueous phase including low acid (0.001 M HNO_3), AOT itself extracted high amount of holmium and water and showed high intensity of spherical aggregates. To compare the MLE and the

shape of different AOT ratio, the P(r) functions of low acid results are normalized in respect to P(r)$_{max}$ and are shown in Fig.8. As the AOT ratio decrease, the peak center shift to lower r which suggest that the CMPO prohibit the formation of large spherical aggregates. When the lowest amount of AOT or no AOT is applied in the mixed system (AOT ratio = 0.2 and 0), it showed a symmetric pronounced peak at low-r regime with a long tail at higher-r regime suggesting spherical shapes coexisting with long rod shapes. It is noteworthy that a second peak appeared, as a shoulder on the first peak, for AOT ratios of 0.8 and 0.5 which may be caused by the attractive interaction between the two different extractants[35, 70]. The 2nd inflection point of those two graphs is at a similar location (~16 Å) but the graphs have different second peak intensity. These results suggest that in both ratios similar cross-sectional dimension shapes are formed but a stronger interaction exist for 1:1 ratio of the extractants, i.e. at an AOT ratio = 0.5.

For the organic phase after contact with higher acid concentration in both 0.5 M and 3 M HNO$_3$, an exponentially decaying length distribution at high r-tail was observed for the AOT ratio of 0.8, 0.5 and 0.2 which suggest typical cylindrical particle feature. However, for the AOT ratio of 0, the results show a pronounced peak at low r-regime with longer tail at higher-r regime which suggest globular shape with some elongated rod shape. The results from the SAXS, as well as the water uptake data, at different acid concentration show that low acid generate extensive aggregate formation using AOT only while at higher acid concentration there is much less tendency to form a microemulsion in the organic phase. The SAXS data still suggest that there is some formation of smaller aggregates even after contact with 3 M HNO$_3$. In our previous studies, we have seen evidence that AOT deform

after contact with higher acid concentration which is likely part of the reason for the

behavior observed here.
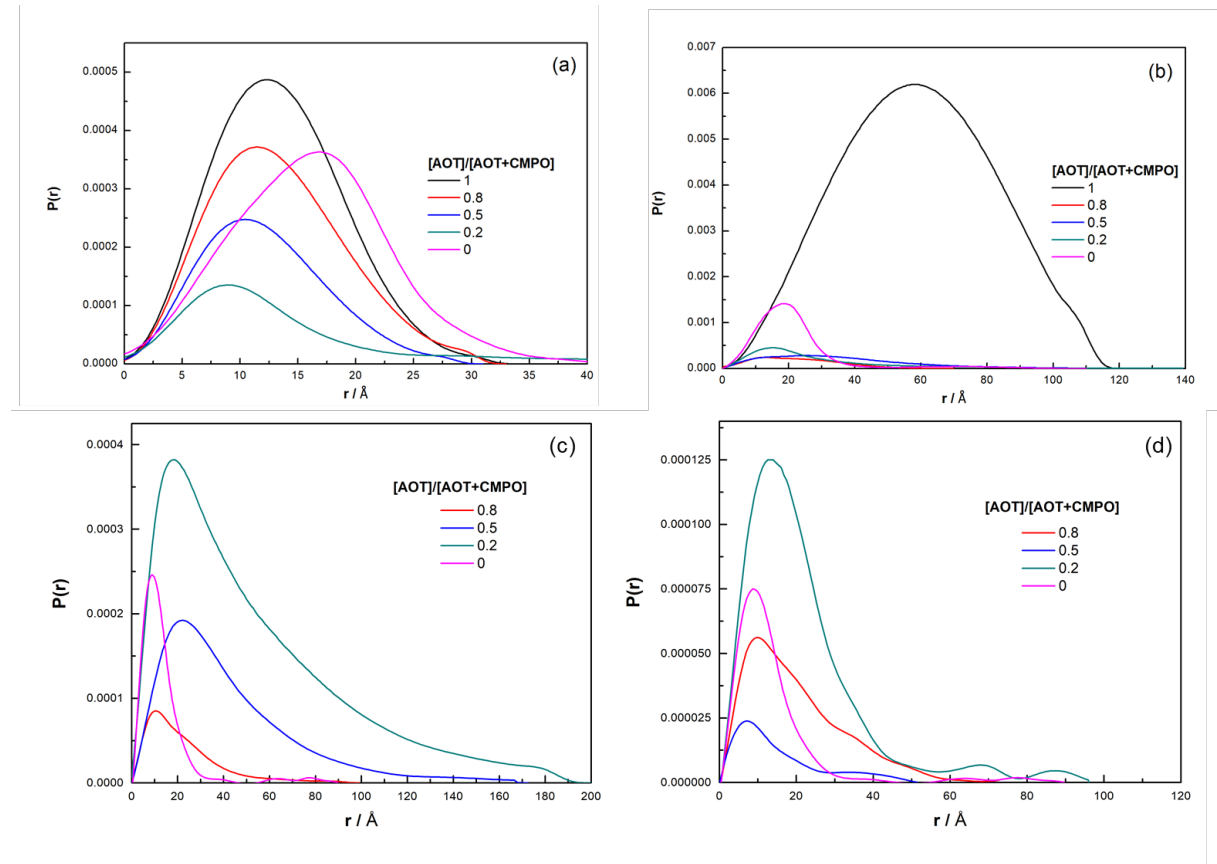
Figure 4.7 P(r) functions for the organic phase (a) before contact with the aqueous phase (b) after contact with the aqueous phase containing 0.01M Ho^{3+} in 0.001M HNO$_3$ acid concentration, (c) after contact with the aqueous phase containing 0.01M Ho^{3+} in 0.5 M HNO$_3$ and (d) after contact with the aqueous phase containing Ho^{3+} in 3 M HNO$_3$ aqueous phase.
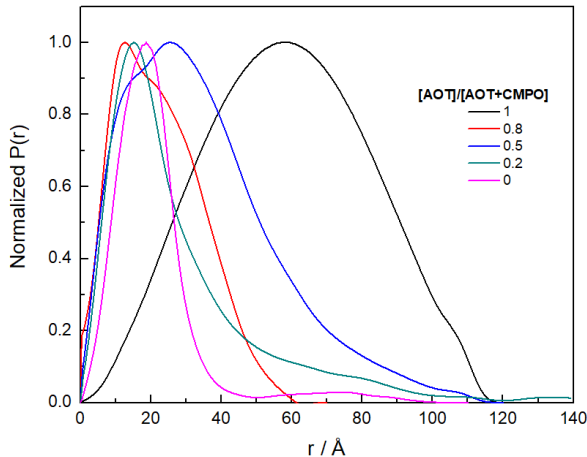
Figure 4.8 Normalized P(r) function for the organic phase after contact with the aqueous phase containing 0.01 M Ho^{3+} in 0.001 M HNO_3 concentration (Normalized P(r) function of Figure 4.7 (b)).

Table 4.3 Maximum linear extent (MLE) and inflection point from the PDDFs (Figure 4.7) for the organic solution before and after contact with the aqueous phase containing 0.01M holmium nitrate in 0.001M HNO_3

	Contacted Acid concentration / M	AOT ratio				
		1	0.8	0.5	0.2	0
MLE / Å	Before contact	34	33	31	47	63
	0.001M	120	70	120	130	120
	0.5M	-	100	170	200	90
	3M	-	72.8	51.4	96	90
Inflection point / Å	Before contact	18.80	17.88	15.97	13.25	22.22
	0.001M	89	16.20	16.44	21.96	25.5
	0.5M	-	14.89	39.38	28.30	14.76
	3M	-	13.40	31.62	19.60	14.77

Our study shows that the distribution ratio increases with the AOT concentration, but the aqueous phase is not stable due to massive production of micelle in the aqueous phase. However, this problem can be solved by adding the CMPO in the organic phase which cause attractive interaction with AOT. The SAXS results in the organic phase before contact with the aqueous phase shows that mixing of the two extractants results in

formation of bigger aggregates, likely due to interaction between the two organic molecules. However, after contact with the aqueous phase, significant rearrangement and attraction effect between AOT and CMPO appeared especially for low acid concentration. As the acid concentration in the aqueous phase increase, the AOT deformation occurred and the attraction between AOT and CMPO decreased resulting in the formation of predominantly cylindrical structures with similar cross-sectional dimension.

4.3 Conclusion

In this chapter, we showed the extractability and morphology change in AOT-CMPO mixed system. From the extractability test, the result shows that AOT itself has good extractability at low acid concentration (0.001 M HNO_3), but the extractability drastically decrease as the acid concentration in the aqueous phase increases. However, when the CMPO is mixed with the AOT system, the extractability did not decrease as drastically compared to AOT itself. In addition, CMPO appear to alleviate the emulsion phase problem of the aqueous phase, possibly due to direct interaction with AOT. SAXS data were collected for all system compositions for the organic phases contacted with different concentration of acidic aqueous solution. In the dry organic phases with mixtures of AOT and CMPO, the data suggested symmetrical spherical aggregates properties, while it showed features suggesting larger aggregate when CMPO was used by itself. After contact with the aqueous phase, a significant reordering occurs in the mixed system. For AOT itself, it showed symmetric spherical aggregates with the largest radius but as the AOT ratio decrease in the mixed system, it formed aggregates of elongated rod shape, and showed an attractive effect between AOT and CMPO through the GIFT-generated P(r) data. In addition to this, we

observed that the degree of reordering decreased upon the concentration of acid in the aqueous phase. We make the observation that for low acid in the aqueous phase there is strong evidence that the extraction synergy correlate with large aggregates in the organic phase. The extractability and structure change observed here may give the evidence of the extraction mechanism with different types of extractants that cause the formation of microemulsions.

CHAPTER 5. SUMMARY AND CONCLUSION

Solvent extraction is a useful technique to separate lanthanides and actinides from a used nuclear fuel waste stream. The technique includes transport of desired solutes between two immiscible aqueous and organic phases using extraction reagents, or extractants. Among the various extractants, surfactants have been studied due to their ability to form reverse micelle. The reverse micellar extraction has a great potential to create a new process of high performance extraction of metal ions. To understand the reverse micellar extraction, Aerosol OT(AOT), which has a double-chain anionic surfactant known to form microemulsion, was adapted as the extractant. AOT extracts lanthanides by ion exchange but it is impractical to use by itself as an extractant due to limited extractability and the formation of excessive emulsion under certain conditions. However, we observed that the extractability and stability of AOT drastically improved with increasing target metal concentration in the aqueous phase. Also, the addition of electrolytes such as sodium nitrate and nitric acid in the aqueous phase can inhibit the third phase formation although the additional acid causes the AOT molecule to become protonated which prevents reverse micelle formation and, by extension, decreases extraction into the organic phase. These results suggest that AOT can have some application as an extractant although its use by itself is limited.

In addition to changing the extraction environment of AOT by different pH or ionic strength of the aqueous phase, the formation of third phase and the poor extractability can be solved by adding a neutral extractant, such as CMPO, to the organic phase. By doing so, the extractability of CMPO is surprisingly enhanced in the AOT-based microemulsion

system compared to CMPO itself. UV-Vis experiments showed that extracted lanthanides by AOT exhibits the same spectra as the lanthanide nitrates in the aqueous phase, which suggest that extracted lanthanides are surrounded by water in the organic phase. However, once CMPO is added into the AOT system, the band shape of the lanthanides changed drastically indicating that the complexation between CMPO and the lanthanides cause a change of the environment around the extracted metal ion. This result was also confirmed though XAFS analysis. To understand the higher coordination shell, we adapted the wavelet transform of the EXAFS spectrum. From this analysis, we observed that CMPO binds with lanthanides to form a complex with bidentate mode with C=O and P=O and decreased the amount of hydrated water around the metal ion. The absorption spectroscopic properties show partially complexed properties when the CMPO is mixed with AOT resulting in a stable organic phase and increased extractability. Also, the macroscopic structural properties were measured for AOT-CMPO mixed system through small angle X-ray scattering (SAXS). In the organic phase before contact with the aqueous phase, the AOT and CMPO shows symmetrical spherical aggregates with features suggesting larger aggregate when CMPO was used by itself. After contact with the aqueous phase a significant reordering was observed, especially for the case of low acid concentration in the aqueous phase. These observations point towards strong evidence that the extraction synergy correlate with large aggregates in the organic phase when using low acid in the aqueous phase. Also, it showed that the CMPO complexation with AOT is aiding the control of water extraction through reverse micelles of AOT which results in the synergistic effect using mixtures of AOT and CMPO.

All in all, our studies show a proof of concept containing the role of reverse micelle and coordination environment of mixed extractants in a solvent extraction system. The reverse micelle can be used as catalyst for the extraction but once the amount of formed reverse micelle increased, it causes excessive amount of unwanted emulsion phase in both aqueous and organic phase. However, the neutral extractant CMPO can solve this problem by coordinating with the reverse micelle resulting in improved extractability. This finding coupled with the various analysis method conducted in this thesis may be applied to other synergistic solvent extraction system and suggest further insight of mixed extractant systems which include surface active reagents. Also, it will provide hints for how to manipulate existing extraction systems to get better output throughout a separation process.

REFERENCES

1. Benedict, M., *Nuclear Chemical Engineering*. McGraw-Hill College: 1981; p 1008.

2. Hill, C. m., Overview of Recent Advances in An(III)/Ln(III) Separation by Solvent Extraction. CRC Press: 2010; Vol. 20096466, pp 119-193.

3. Konings, R. J. M.; Allen, T. R.; Stoller, R. E.; Yamanaka, S., *Comprehensive Nuclear Materials*. 2012.

4. Haque, N.; Hughes, A.; Lim, S.; Vernon, C., Rare Earth Elements: Overview of Mining, Mineralogy, Uses, Sustainability and Environmental Impact. *Resources* **2014,** *3*, 614-635.

5. Wall, F., Rare earth elements. John Wiley & Sons: Oxford, 2013; Vol. 89, pp 312-339.

6. Zepf, V., Rare Earth Elements: What and Where They Are. Springer Berlin Heidelberg: Berlin, Heidelberg, 2013; pp 11-39.

7. England, T. R.; Rider, B. F. *Evaluation and compilation of fission product yields 1993*; Dec 31, 1995.

8. Nash, K. L.; Lumetta, G. J., *Advanced Separation Techniques for Nuclear Fuel Reprocessing and Radioactive Waste Treatment*. Elsevier: 2011; p 512.

9. Horwltz, E. P.; Martin, K. A.; Diamond, H.; Kaplan, L., EXTRACTION OF Am FROM NITRIC ACID BY CARBAMOYL-PHOSPHORYL EXTRACTANTS: THE INFLUENCE OF SUBSTITUENTS ON THE SELECTIVITY OF Am OVER Fe AND SELECTED FISSION PRODUCTS. *Solvent Extraction and Ion Exchange* **1986,** *4*, 449-494.

10. Goklen, K. E.; Hatton, T. A., Liquid-Liquid Extraction of Low Molecular-Weight Proteins by Selective Solubilization in Reversed Micelles. *Separation Science and Technology* **1987,** *22*, 831-841.

11. Melo, E. P.; Aires-Barros, M. R.; Cabral, J. M. S., Reverse micelles and protein biotechnology. Elsevier: 2001; Vol. 7, pp 87-129.

12. Szymanowski, J.; Tondre, C., KINETICS AND INTERFACIAL PHENOMENA IN CLASSICAL AND MICELLAR EXTRACTION SYSTEMS. *Solvent Extraction and Ion Exchange* **1994,** *12*, 873-905.

13. Malik, M. A.; Wani, M. Y.; Hashim, M. A., Microemulsion method: A novel route to synthesize organic and inorganic nanomaterials. *Arabian Journal of Chemistry* **2012,** *5*, 397-417.

14. Naganawa, H.; Suzuki, H.; Tachimori, S., Cooperative effect of carbamoylmethylene phosphine oxide on the extraction of lanthanides(III) to water-in-oil microemulsion from concentrated nitric acid medium. *Physical Chemistry Chemical Physics* **2000,** *2*, 3247-3253.

15. Rydberg, J., *Solvent Extraction Principles and Practice, Revised and Expanded*. CRC Press: 2004; p 480.

16. Osseo-Asare, K., Aggregation, reversed micelles, and microemulsions in liquid-liquid extraction: the tri-n-butyl phosphatediluent-water-electrolyte system. *Advances in Colloid and Interface Science* **1991,** *37*, 123-173.

17. Preston, J. S.; du Preez, A. C., SOLVENT EXTRACTION OF URANIUM(VI) AND THORIUM(IV) FROM NITRATE MEDIA BY CARBOXYLIC ACID AMIDES. *Solvent Extraction and Ion Exchange* **1995,** *13*, 391-413.

18. Otu, E. O.; Chiarizia, R.; Rickert, P. G.; Nash, K. L., The Extraction of Americium and Strontium by P,P′-Di(2-Ethylhexyl) Benzene-1,2-Diphosphonic acid. *Solvent Extraction and Ion Exchange* **2007,** *20*, 607-632.

19. Buch, A.; Stambouli, M.; Pareau, D.; Durand, G., SOLVENT EXTRACTION OF NICKEL(II) BY MIXTURE OF 2-ETHYLHEXANAL OXIME AND BIS(2-ETHYLHEXYL) PHOSPHORIC ACID. *Solvent Extraction and Ion Exchange* **2002,** *20*, 49-66.

20. Jensen, M. P.; Bond, A. H., Influence of aggregation on the extraction of trivalent lanthanide and actinide cations by purified Cyanex 272, Cyanex 301, and Cyanex 302. *Radiochimica Acta* **2002,** *90*, 145.

21. Thiyagarajan, P.; Diamond, H.; Horwitz, E. P., Small-angle neutron scattering studies of the aggregation of Pr(NO 3) 3–CMPO and PrCl 3–CMPO complexes in organic solvents. *Journal of Applied Crystallography* **1988,** *21*, 848-852.

22. Diamond, H.; Thiyagarajan, P.; Honvitz, E. P., SMALL ANGLE NEUTRON SCATTERING STUDIES OF PRASEODYMIUM-CMPO POLYMERIZATION H. *Solvent Extraction and Ion Exchange* **1990,** *8*, 503-513.

23. Jensen, M. P.; Chiarizia, R.; Urban, V., Investigation of the Aggregation of the Neodymium complexes of Dialkylphosphoric, -Oxothiophosphinic, and -Dithiophosphinic acids in Toluene. *Solvent Extraction and Ion Exchange* **2001,** *19*, 865-884.

24. Chiarizia, R.; Jensen, M. P.; Rickert, P. G.; Kolarik, Z.; Borkowski, M.; Thiyagarajan, P., Extraction of Zirconium Nitrate by TBP in n-Octane: Influence of Cation Type on Third Phase Formation According to the "Sticky Spheres" Model. *Langmuir* **2004,** *20*, 10798-10808.

25. Sathyanarayana, D. N., *Electronic Absorption Spectroscopy and Related Techniques*. Universities Press: 2001; p 532.

26. Cotton, S., *Lanthanide and Actinide Chemistry*. John Wiley & Sons: 2013; p 272.

27. Denning, R. G., Electronic Structure and Bonding in Actinyl Ions and their Analogs. *The Journal of Physical Chemistry A* **2007,** *111*, 4125-4143.

28. Thompson, M. C. *Demonstration of the UREX Solvent Extraction Process with Dresden Reactor Fuel Solution*; Nov 01, 2002.

29. Karraker, D. G., Coordination of trivalent lanthanide ions. *Journal of Chemical Education* **1970,** *47*, 424.

30. Judd, B. R., Hypersensitive Transitions in Rare- Earth Ions. *The Journal of Chemical Physics* **1966,** *44*, 839-840.

31. Chrissanthopoulos, A.; Papatheodorou, G. N., Temperature dependence of the f←f hypersensitive transitions of Ho3+ and Nd3+ in molten salt solvents and the structure of the LaCl3–KCl melts. *Journal of Molecular Structure* **2006,** *782*, 130-142.

32. Karraker, D. G., Hypersensitive transitions of six-, seven-, and eight-coordinate neodymium, holmium, and erbium chelates. *Inorganic Chemistry* **1967,** *6*, 1863-1868.

33. Glatter, O.; Fritz, G.; Lindner, H.; Brunner-Popela, J.; Mittelbach, R.; Strey, R.; Egelhaaf, S. U., Nonionic micelles near the critical point: Micellar growth and attractive interaction. *Langmuir* **2000,** *16*, 8692-8701.

34. Ilavsky, J.; Jemian, P. R., Irena: tool suite for modeling and analysis of small-angle scattering. *Journal of Applied Crystallography* **2009,** *42*, 347-353.

35. Shrestha, L. K.; Sato, T.; Aramaki, K., Phase Behavior and Self-Organized Structures of Diglycerol Monolaurate in Different Nonpolar Organic Solvents. *Langmuir* **2007,** *23*, 6606-6613.

36. Shrestha, L. K.; Glatter, O.; Aramaki, K., Structure of Nonionic Surfactant (Glycerol α-Monomyristate) Micelles in Organic Solvents: A SAXS Study. *The Journal of Physical Chemistry B* **2009,** *113*, 6290-6298.

37. Koningsberger, D. C.; Mojet, B. L.; van Dorssen, G. E.; Ramaker, D. E., XAFS spectroscopy; fundamental principles and data analysis. *Topics in Catalysis* **2000,** *10*, 143-155.

38. Koningsberger, D. C.; Prins, R., *X-ray absorption: principles, applications, techniques of EXAFS, SEXAFS, and XANES.* John Wiley and Sons,New York, NY: United States, 1988.

39. Jugnet, Y.; Grenet, G.; Duc, T. M., CHAPTER 10 - SURFACE CORE LEVEL SHIFT. In *Handbook on Synchrotron Radiation*, Marr, G. V., Ed. Elsevier: Amsterdam, 1987; pp 663-722.

40. Fritz, G.; Bergmann, A.; Glatter, O., Evaluation of small-angle scattering data of charged particles using the generalized indirect Fourier transformation technique. *The Journal of Chemical Physics* **2000,** *113*, 9733-9740.

41. Yukselen, M. A.; Gregory, J., The effect of rapid mixing on the break- up and re-formation of flocs. *Journal of Chemical Technology & Biotechnology* **2004,** *79*, 782-788.

42. Malbrel, C. A.; Somasundaran, P., Water-induced dispersion/flocculation of colloidal suspensions in nonpolar media. *Journal of Colloid and Interface Science* **1989,** *133*, 404-408.

43.   Moon, J.; Nilsson, M., Investigation on the Properties of Micelle and Reverse Micelle in Water/AOT/Heptane system for Holmium Extraction. In *Proceddings of GLOBAL, International Nuclear fuel cycle conference*, Seoul, South Korea, 2017.

44.   Domínguez, A.; Fernández, A.; Gonzalez, N.; Iglesias, E.; Montenegro, L., Determination of critical micelle concentration of some surfactants by three techniques. *Journal of Chemical Education* **1997,** *74*, 1227-1231.

45.   Izutsu, K., *Electrochemistry in Nonaqueous Solutions*. WILEY-VCH Verlag GmbH & Co: Weinheim, 2009.

46.   Sjoblom, J., *Emulsions and Emulsion Stability*. CRC Press: 2005; p 688.

47.   Glatter, O.; Fritz, G.; Lindner, H.; Brunner-Popela, J.; Mittelbach, R.; Strey, R.; Egelhaaf, S. U., Nonionic Micelles near the Critical Point: Micellar Growth and Attractive Interaction. *Langmuir* **2000,** *16*, 8692-8701.

48.   Hirai, M.; Kawai-Hirai, R.; Takizawa, T.; Yabuki, S.; Nakamura, K.; Hirai, T.; Kobayashi, K.; Amemiya, Y.; Oya, M., Aerosol-OT Reversed Micellar Formation at Low Water-Surfactant Ratio Studied by Synchrotron Radiation Small-Angle X-ray Scattering. *The Journal of Physical Chemistry* **1995,** *99*, 6652-6660.

49.   HIRAI, M.; KAWAIHIRAI, R.; HIRAI, T.; UEKI, T., Structural-Change of Jack Bean Urease Induced by Addition of Surfactants Studied with Synchrotron-Radiation Small-Angle X-Ray-Scattering. *European Journal of Biochemistry* **1993,** *215*, 55-61.

50.   Fathi, H.; Kelly, J. P.; Vasquez, V. R.; Graeve, O. A., Ionic Concentration Effects on Reverse Micelle Size and Stability: Implications for the Synthesis of Nanoparticles. *Langmuir* **2012,** *28*, 9267-9274.

51. Suzuki, H.; Naganawa, H.; Tachimori, S., Extraction of Europium(III) into W/O Microemulsion Containing Aerosol OT and a Bulky Diamide. I. Cooperative Effect. *Solvent Extraction and Ion Exchange* **2003,** *21*, 527-546.

52. Karraker, D. G., Hypersensitive transitions of hydrated neodymium-(III)holmium-(III) and erbium-(III) ions. *Inorganic Chemistry* **2002,** *7*, 473-479.

53. Gullekson, B. J.; Breshears, A. T.; Brown, M. A.; Essner, J. B.; Baker, G. A.; Walensky, J. R.; Paulenova, A.; Gelis, A. V., Extraction of Water and Speciation of Trivalent Lanthanides and Americium in Organophosphorus Extractants. *Inorganic Chemistry* **2016,** *55*, 12675-12685.

54. Muñoz, M.; Farges, F.; Argoul, P., Continuous Cauchy wavelet transform of XAFS spectra. *Physica Scripta* **2005,** *2005*, 221.

55. Funke, H.; Scheinost, A. C.; Chukalina, M., Wavelet analysis of extended x-ray absorption fine structure data. *Physical Review B* **2005,** *71*, 094110.

56. Shao, L.; Lin, X.; Shao, X., A WAVELET TRANSFORM AND ITS APPLICATION TO SPECTROSCOPIC ANALYSIS. *Applied Spectroscopy Reviews* **2002,** *37*, 429-450.

57. Kropf, A. J.; Katsoudas, J.; Chattopadhyay, S.; Shibata, T.; Lang, E. A.; Zyryanov, V. N.; Ravel, B.; McIvor, K.; Kemner, K. M.; Scheckel, K. G.; Bare, S. R.; Terry, J.; Kelly, S. D.; Bunker, B. A.; Segre, C. U., The New MRCAT (Sector 10) Bending Magnet Beamline at the Advanced Photon Source. *AIP Conference Proceedings* **2010,** *1234*, 299-302.

58. Ravel, B.; Newville, M., ATHENA, ARTEMIS, HEPHAESTUS: data analysis for X-ray absorption spectroscopy using IFEFFIT. *Journal of Synchrotron Radiation* **2005,** *12*, 537-541.

59. Timoshenko, J.; Kuzmin, A.; Purans, J., EXAFS study of hydrogen intercalation into ReO 3 using the evolutionary algorithm. *Journal of Physics: Condensed Matter* **2014,** *26*, 055401.

60. Koma, Y.; Watanabe, M.; Nemoto, S.; Tanaka, Y., Trivalent f-element intra-group separation by solvent extraction with cmpo-complexant system. *Journal of Nuclear Science and Technology* **1998,** *35*, 130-136.

61. Delmau, L. H.; Simon, N.; Schwing-Weill, M.-J.; Arnaud-Neu, F.; Dozol, J.-F.; Eymard, S.; Tournois, B.; Grüttner, C.; Musigmann, C.; Tunayar, A.; Böhmer, V., EXTRACTION OF TRIVALENT LANTHANIDES AND ACTINIDES BY "CMPO-LIKE" CALIXARENES. *Separation Science and Technology* **1999,** *34*, 863-876.

62. Bera, M. K.; Luo, G.; Schlossman, M. L.; Soderholm, L.; Lee, S.; Antonio, M. R., Erbium(III) Coordination at the Surface of an Aqueous Electrolyte. *The Journal of Physical Chemistry B* **2015,** *119*, 8734-8745.

63. Chaiko, D. J.; Fredrickson, D. R.; Reichley-yinger, L.; Vandegrift, G. F., Thermodynamic Modeling of Chemical Equilibria in Metal Extraction. *Separation Science and Technology* **1988,** *23*, 1435-1451.

64. Tkac, P.; Vandegrift, G. F.; Lumetta, G. J.; Gelis, A. V., Study of the Interaction between HDEHP and CMPO and Its Effect on the Extraction of Selected Lanthanides. *Industrial & Engineering Chemistry Research* **2012,** *51*, 10433-10444.

65. Fei, H.; Dong, J.; Arellano-Jiménez, M. J.; Ye, G.; Dong Kim, N.; Samuel, E. L. G.; Peng, Z.; Zhu, Z.; Qin, F.; Bao, J.; Yacaman, M. J.; Ajayan, P. M.; Chen, D.; Tour, J. M., Atomic cobalt on nitrogen-doped graphene for hydrogen generation. *Nature Communications* **2015,** *6*, 8668.

66. Rehr, J. J.; Kas, J. J.; Prange, M. P.; Sorini, A. P.; Takimoto, Y.; Vila, F., Ab initio theory and calculations of X-ray spectra. *Comptes Rendus Physique* **2009,** *10*, 548-559.

67. Fujii, T.; Aoki, K.; Yamana, H., Effect of Nitric Acid Distribution on Extraction Behavior of Trivalent F- Elements in a TRUEX System. *Solvent Extraction and Ion Exchange* **2006,** *24*, 347-357.

68. Spencer Barry, B.; Counce Robert, M.; Egan, B. Z., Extraction of nitric acid from aqueous media with OϕD(iB)CMPO–n-dodecane. *AIChE Journal* **2004,** *43*, 555-564.

69. Shrestha, L. K.; Sharma, S. C.; Sato, T.; Glatter, O.; Aramaki, K., Small-angle X-ray scattering (SAXS) study on nonionic fluorinated micelles in aqueous system. *Journal of Colloid and Interface Science* **2007,** *316*, 815-824.

70. Ellis, R. J.; Anderson, T. L.; Antonio, M. R.; Braatz, A.; Nilsson, M., A SAXS Study of Aggregation in the Synergistic TBP–HDBP Solvent Extraction System. *The Journal of Physical Chemistry B* **2013,** *117*, 5916-5924.